Densification and Recrystallization of Firn At Dome C, Central East Antarctica

A Senior Honors Thesis

Presented in Partial Fulfillment of the Requirements for graduation **with distinction in Geology and Mineralogy** in the undergraduate colleges of The Ohio State University

by

Richard Alley

The Ohio State University
June 1980

Project Adviser: Professor Ian Whillans, Department of Geological Sciences

DENSIFICATION AND RECRYSTALLIZATION OF FIRN AT DOME C, CENTRAL EAST ANTARCTICA

by

Richard B. Alley

DENSIFICATION AND RECRYSTALLIZATION OF FIRN AT DOME C, CENTRAL EAST ANTARCTICA

Senior Thesis

The Ohio State University
Department of Geology and Mineralogy

Spring, 1980

Presented
in partial fulfillment
of the requirements
for the degree
Bachelor of Science
with distinction

by

Richard B. Alley

Approved

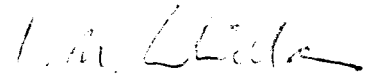

Dr. Ian M. Whillans,
adviser.

ABSTRACT. A study of variations of density, crystal size, and crystal shape with depth to 50 m depth for Dome C, central East Antarctica, is reported.

The critical point in the depth-density profile is less sharply defined than at many locations. Benson's model for variation of pore space with depth provides an adequate, but not perfect, description of the observed behavior. An empirical relation discovered by Gow for dependence of depth-density profiles on temperature and accumulation cannot be extended to the low-temperature, low-accumulation conditions of Dome C.

The observed profile differs from log-linear densification expected for unconfined sintering of ceramics in a manner which is explicable if load has an important effect on densification. The relative behavior of the Dome C and South Pole age-density profiles also shows that load is an important parameter in firn densification.

The core consists of dense, fine-grained wind crusts contained in more-extensive, less-dense, coarse-grained firn. Density ranges between superjacent coarse and fine layers decrease exponentially with depth. Lower rates of densification are observed for fine-grained firn because such firn has greater area of grain boundary per unit volume than coarse firn, and so resists deformation under load better. A simple unconfined-sintering model for densification predicts more rapid densification of fine firn, and thus is shown to have limited applicability.

Load and mean annual temperature are probably the controlling factors in firn densification between 5 m and 50 m depth.

The rate of growth of crystals in fine layers is almost three times that of crystals in coarse layers. The rate of growth of coarse crystals agrees well with that predicted by Gow. Variations in crystal sphericity, internal free surface, and crystal boundary area with depth reveal that coarse-grained firn consists of several genetically-different types of firn.

Thin sections of firn may be prepared using the nontoxic chemical dodecane as a filler. To determine mean crystal area in a section, the 50 largest crystals following the 5 largest crystals should be measured, such that about 25% of the crystals in a section are measured.

ACKNOWLEDGEMENTS

This study would not have been possible without the help of many people. Ron Coffman, Julie Palais, and John Bolzan gave valuable information and advice, and Ron's mechanical wizardry proved very useful. Dr. David H. Elliot and Dr. Garry McKenzie helped in the formulation of the problems. Dr. S. Leslie Blatt and Dean Colin Bull of the honors reading committee provided many helpful suggestions. Cindy Richardson provided insight, and much-needed moral support.

The project was funded by an Undergraduate Research Scholarship administered by the O.S.U. College of the Arts and Sciences Honors Office, and was also funded by Dr. Ian Whillans from National Science Foundation Division of Polar Programs grant 76-23428. The Institute of Polar Studies and the Department of Geology and Mineralogy supplied much material support.

Most of all, I am indebted to my adviser, Ian Whillans, for providing ideas, guidance, samples, funds, and enough advice to see this study through to a successful conclusion.

TABLE OF CONTENTS

LIST OF APPENDICES

LIST OF FIGURES

INTRODUCTION

Studies of the transformation of snow to firn and then to ice on high polar glaciers have been conducted for many locations in recent years. This process has been variously described as sintering (Gow, 1968), metamorphism (Bader and others, 1939), and diagenesis (Paulcke, 1934). It includes both densification and recrystallization.

Much of the work in the field has been of an empirical nature. Papers by Gow have established a coherent picture of the data collected regarding densification (1968, 1974) and recrystallization (1969), and provide an excellent framework against which new studies, including this one, can be evaluated.

Data collected and reviewed by Gow cover locations with mean annual temperatures of $-17^{\circ}C$ (Base Roi Baudouin, Tongiori and others, 1962) to $-51^{\circ}C$ (South Pole, Giovinetto, 1960), and mean annual accumulations of 410 kg m^{-2} a^{-1} (Roi Baudouin) to 70 kg m^{-2} a^{-1} (South Pole). However, except for limited work at Plateau Station (Koerner and Kane, 1967) and work in progress at Vostok Station (Korotkevitch and others, 1978), no attempts have been made to extend Gow's work to colder, lower accumulation regions. This paper does so.

Studies of this sort have potential applications in other areas of glaciology. Interpretation of gas-content measurements of glacier ice may be further refined if densification and recrystallization in firn are better understood (Raynaud, 1976). Interpretation of heat conduction also depends on knowledge of firn structure (Lax, 1978).

Models of microwave emission from polar ice caps indicate that the observed emission patterns depend in part on grain sizes and their variation with depth (Chang, 1976; Zwally, 1977). Information from new areas, such as Dome C, should help in understanding and interpreting microwave emissions.

CORE DESCRIPTION

Dome C is an ice divide located at 74° 39' S latitude and 124° 10' E longitude, at an elevation of 3,240 m. Duval and Lorius (in press) report a mean annual temperature of -53.5°C, but recent measurements (Bolzan, private communication, 1980) indicate that -54.3°C may be a better value for the 10 m firn temperature. The mean annual accumulation is 34 kg m^{-2} a^{-1} (Palais, 1980).

A 50 m ice core was drilled there during the 1978-79 austral summer by personnel from the Polar Ice Coring Office, Lincoln, Nebraska. The 75 mm diameter core was shipped to Columbus, Ohio where it was studied during the fall and winter of 1979-80.

Examination of the core in transmitted light revealed distinct layering. Individual layers range from 1 mm to several tens of millimeters in thickness. The core is mainly composed of coarse firn with high light transmissivity, but contains thin, fine-grained, low-transmissivity layers. Contacts between layers are abrupt. Although more distinct at the surface, layers are still well-defined at 50 m. At no point is there any indication of a regular spacing corresponding to annual layering, or any other regularity. Small variations in transmissivity and grain size reveal layers within the coarse firn.

The variations are not sufficiently large to allow the distinction and classification of different types of coarse firn.

The form of the fine, dark layers is suggestive of an aeolian origin. Many of these layers vary in thickness across the width of the core. One layer in particular, at about 4.5 m depth, thinned from 25 mm to less than 5 mm thick across the core diameter. This indicates that many of the features seen as layers in the core are actually lenses of limited extent. Nonetheless, the term layer will be retained for distinct units of firn in the core with abrupt and approximately horizontal boundaries.

Palais (1980) conducted detailed pit studies at Dome C. She found fine-grained, discontinuous crusts of limited thickness and lateral extent, contained in coarser, more extensive firn. She interpreted these crusts as having been formed at the surface in late summer. The coarse firn was interpreted to have been deposited during the fall, winter, and spring, and includes genetically distinct depth hoar, soft snow, and intermediate snow. Because of the discontinuous nature of the strata, Palais had difficulty in identifying annual layering in pit walls. It would be even more difficult to correctly and consistently identify annual layering in a single small core. Thus, the features observed in the core are very similar to those expected according to Palais.

DENSITY MEASUREMENTS

--METHOD

Densities were determined by measuring the mass of each sample on a balance, and calculating sample volume from measurements of length and diameter. Entire 1 m core sections were measured where possible. Smaller samples, roughly 20 mm thick, were cut at more-or-less regular intervals along the core, without regard to visible structures. These samples are hereafter referred to as random samples. Finally, other small samples were collected from some core sections to estimate the density range at a given depth. The two adjacent layers in a core section showing the greatest visible contrast were sampled and their densities determined. Experiment showed that density and visible differences are closely correlated, and that density ranges calculated in this manner do approach closely the maximum density ranges in 1 m core sections. Densities above 3 m were measured in deep pits (Palais, 1980). Methods and errors for density measurements, and all other measurements, are discussed more fully in Appendix A.

--DEPTH-DENSITY PROFILE

All of the density data collected are shown in figure 1, and are listed in Appendix B, tables 1, 2, and 3. The

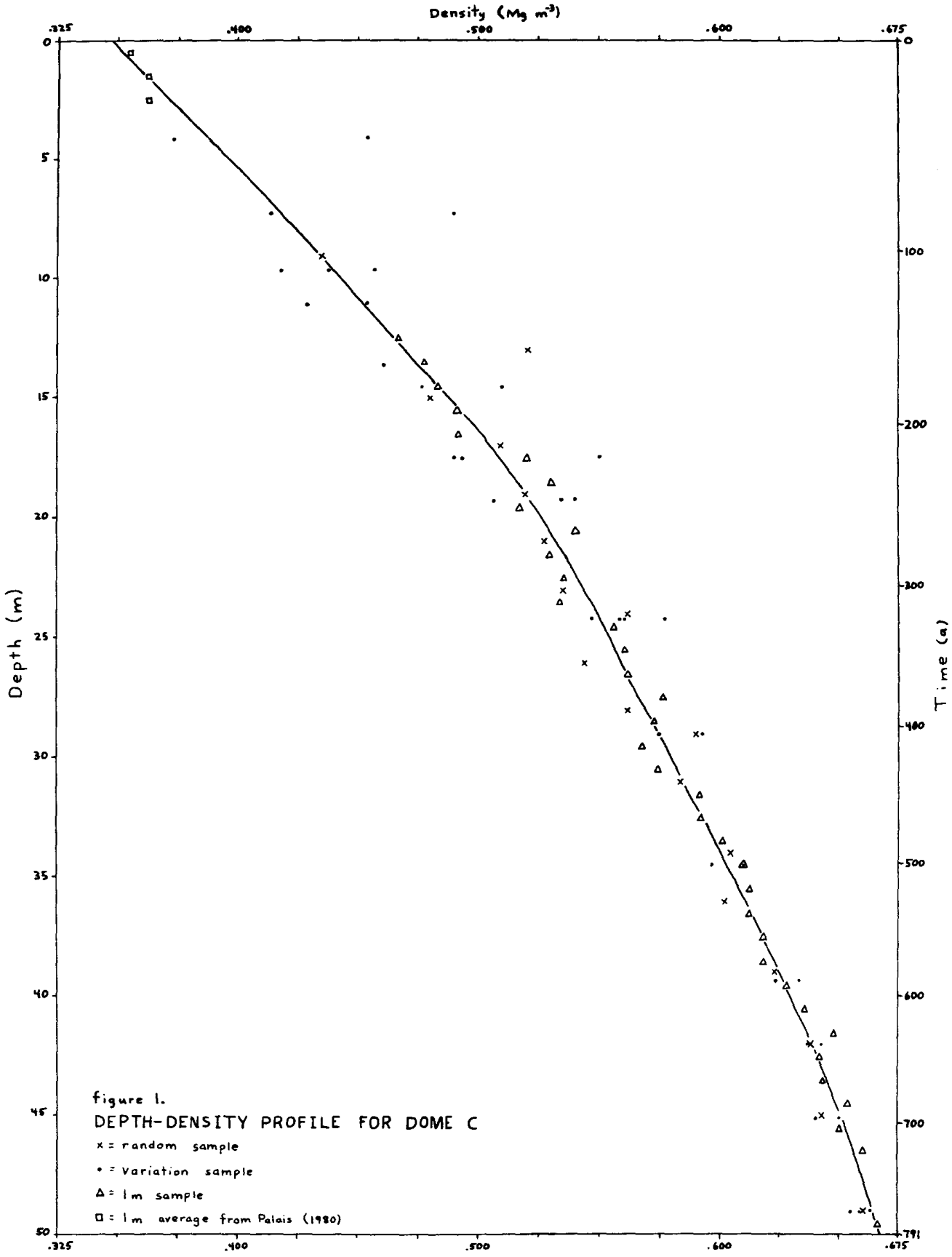

figure 1.

DEPTH-DENSITY PROFILE FOR DOME C

× = random sample

• = variation sample

Δ = 1m sample

□ = 1m average from Palais (1980)

smoothed curve shown in figure 1 was drawn by inspection. Small systematic differences exist between the different density measurement methods used, but these do not significantly affect the values or the form of the curve. The scatter of data about the smoothed curve is due to localized density variations, as well as measurement error. The curve is probably accurate to within 1% or 2%.

The age of firn at each depth was calculated assuming a constant accumulation rate of 34 kg m^{-2} a^{-1} and the smoothed depth-density profile. Ages are also shown in figure 1. Numerical values for the smoothed curve with ages are listed in Appendix B, table 4.

--CRITICAL POINT

Benson (1962) observed that depth-density profiles may be approximated by two line segments of different slopes, intersecting at a density of between 0.50 and 0.55 Mg m^{-3}. He called this the "critical point", and called the depth and density at this point the critical depth and critical density. The critical point in the Dome C depth-density profile is less clearly defined than for many locations, but appears to occur at about 0.510 Mg m^{-3} density and 17.5 m depth.

Benson (1962) related critical density to mean annual temperature for a variety of locations with the empirical equation:

$$\rho_c=\rho_{cl}+(\rho_{co}-\rho_{cl})\exp(ST_c) \qquad (1)$$

in which ρ_c is the critical density and S, ρ_{co}, and ρ_{cl} are the constants:

$$\rho_{cl}=0.50 \text{ Mg m}^{-3}$$
$$\rho_{co}=0.73 \text{ Mg m}^{-3}$$
$$S=0.07^{\circ}C^{-1}$$

and T_c is the temperature at the critical point in $^{\circ}C$. For Dome C, with a temperature of $-54.3^{\circ}C$, this forecasts a critical density of about 0.505 Mg m^{-3}, which is consistent with the observed value.

--LOAD-SPECIFIC VOLUME PROFILE

In order to describe the depth-dependence of density in firn, Benson (1962) assumed that the rate at which pore space is eliminated is related linearly to the pore space present. This gives:

$$\frac{dV_p}{dS}=-mV_p \qquad (2a)$$

or

$$\frac{dV_p}{dS}=-m(V-V_i) \qquad (2b)$$

where the specific volume, V, is defined as the inverse of density, V_i is the specific volume for ice (1.09 m^3 Mg^{-1}), V_p is the volume of pore space ($V_p=V-V_i$), S is the load at depth z below the snow surface, and m is a function of the mechanism of compaction, and includes time-dependent and stress-dependent terms. Benson assumed that m is a constant above the critical point, and a different constant below the critical point.

Equation 2 may be solved for V in terms of S to obtain:

$$V=V_i+(V_o-V_i)\exp(-mS) \qquad (3)$$

where V_o is the specific volume when S=0.

Values for V_o and m must be determined for the two curve sections above and below the critical point. V_o may be obtained by extrapolating a load-specific volume profile to S=0. Observed load and specific volume values for a single point near the midpoint of a curve section may then be substituted into equation 3, and the equation solved for m.

The best fit of Benson's model to the smoothed observed load-specific volume profile for Dome C is obtained with the following values:

Load ($N\ m^{-2}$)	m ($m^2\ N^{-1}$)	V_o ($Mg\ m^{-3}$)
$0-0.7\times10^5$	1.080×10^5	2.86
$0.7\times10^5-2.7\times10^5$	0.389×10^5	2.20

Plots of the calculated and observed load-specific volume profiles are shown in figure 2; data are in Appendix B, table 5.

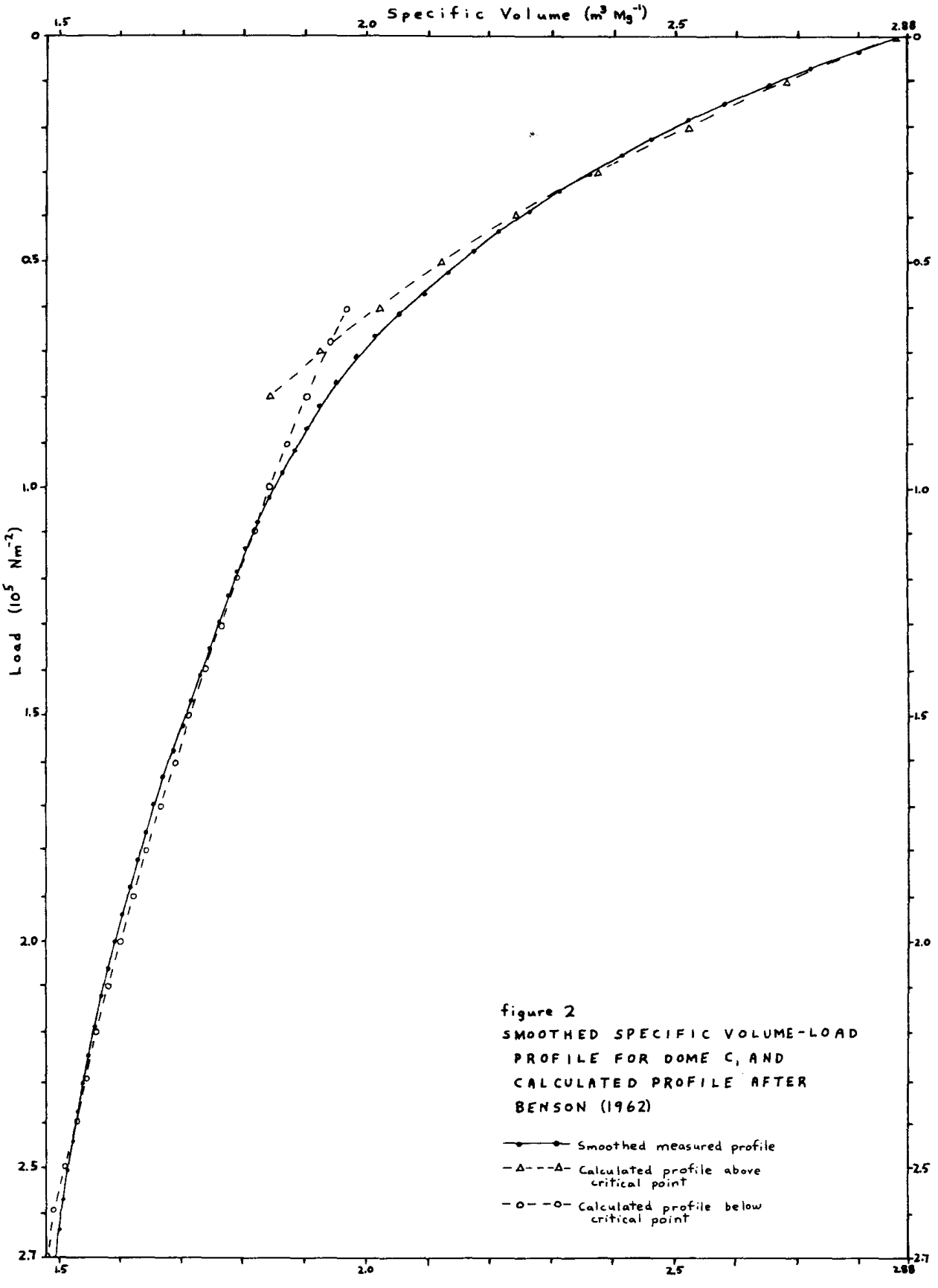

figure 2
SMOOTHED SPECIFIC VOLUME-LOAD PROFILE FOR DOME C, AND CALCULATED PROFILE AFTER BENSON (1962)

—●— Smoothed measured profile

—Δ---Δ— Calculated profile above critical point

—o---o— Calculated profile below critical point

As a rough approximation, the calculated and observed load-specific volume profiles agree well, but there are significant differences. The greatest deviation between the two occurs near the critical point. This may be due, in part, to the method used in drawing the smoothed depth-density profile, from which the load-specific volume profile was calculated. However, it is clear that some deviation exists beyond this possible error. Either m is not quite constant, or the change in pore volume with respect to load deviates slightly from a linear relation to pore volume. These possibilities cannot be distinguished at this time.

--SOUTH POLE versus DOME C DEPTH-DENSITY PROFILES

Gow (1968) compared depth-density profiles from many locations with different rates of accumulation and mean annual temperatures. He found that two locations will have similar depth-density profiles if one has one-half the mean annual accumulation of the other, and has a mean annual temperature $4^{\circ}C$ cooler than the other, and these conditions have been constant over the time when the firn of interest was deposited and subsequently densified.

At South Pole, the coldest, lowest accumulation site considered by Gow, the mean annual temperature is $-50.9^{\circ}C$

and the mean annual accumulation is about 70 kg m^{-2} a^{-1} (Giovinetto, 1960). Dome C has a temperature of -54.3°C and an accumulation rate of 34 kg m^{-2} a^{-1}. According to the relationship suggested by Gow, Dome C and South Pole should have similar depth-density profiles.

The depth-density profiles are compared in figure 3. The smoothed curve for South Pole was drawn by inspection of data from Giovinetto (1960). It is clear that the profiles are significantly different. Also, the firn-ice transition at about 0.830 Mg m^{-3} density is estimated to occur at 110 m depth for South Pole (Gow, 1969), but is observed at 100 m depth for Dome C (Raynaud and others, in press).

The difference between the two profiles indicates either that the measured climatic parameters at at least one of the two sites did not apply during much of the firnification process, or that the relation suggested by Gow cannot be extended to the conditions at Dome C.

Higher temperatures and lower accumulation rates cause more rapid densification with depth. The observed difference between the two profiles might have been caused by a recent decrease in temperature or an increase in accumulation at South Pole, or by an increase in temperature or a decrease in accumulation at Dome C. The empirical relation

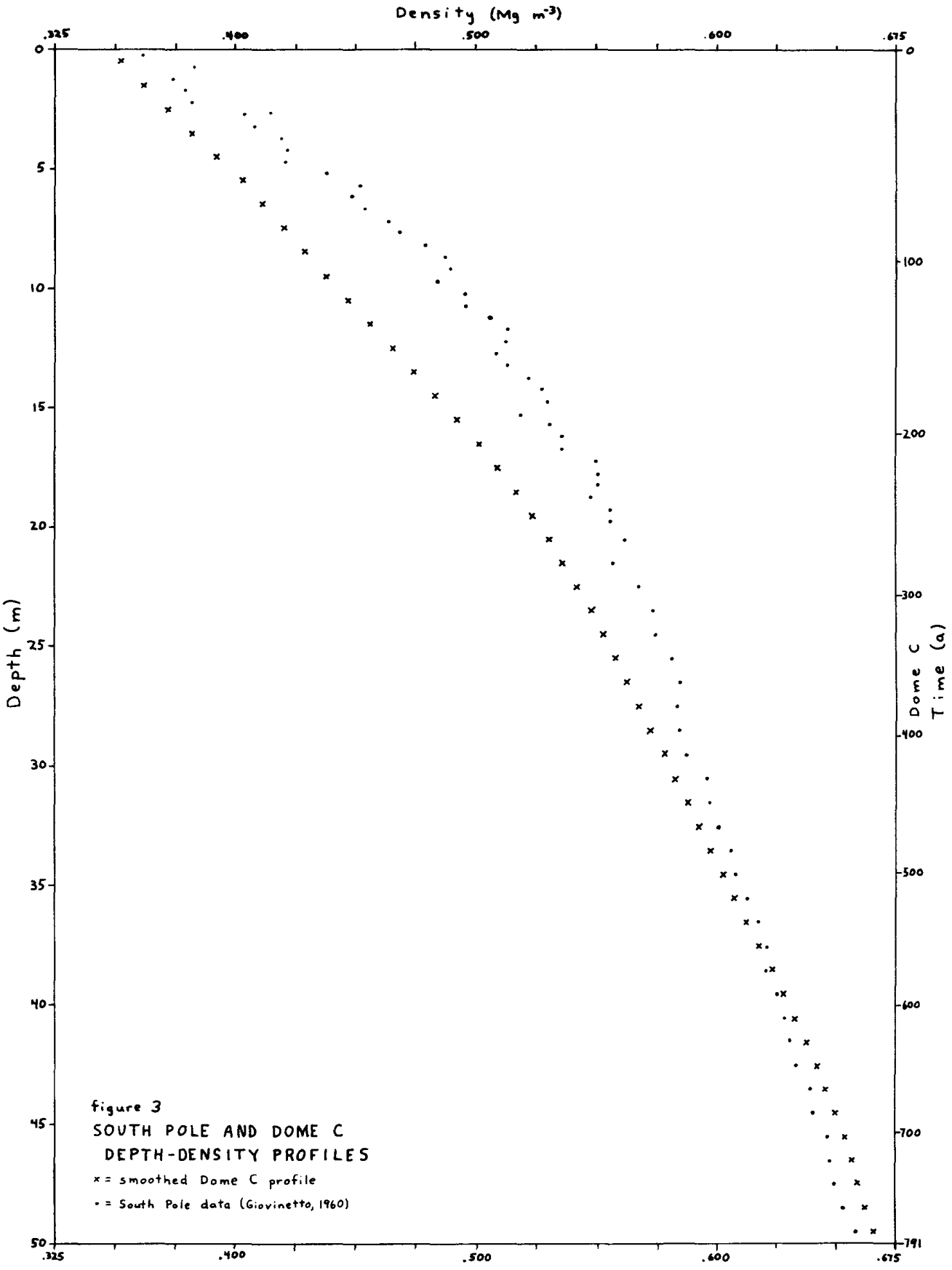

figure 3
SOUTH POLE AND DOME C
DEPTH-DENSITY PROFILES
× = smoothed Dome C profile
· = South Pole data (Giovinetto, 1960)

discovered by Gow does not allow a quantitative consideration of these changes, but a total change (Dome C + South Pole) of at least 2°C or 50% accumulation would probably be required.

Based on microparticle concentrations in a 101 m long core from South Pole, Thompson (1979) reported that the mean annual accumulation for the last 911 a is 69.5 kg m^{-2} a^{-1}, in close agreement with the value determined by visible stratigraphy (Giovinetto, 1960; Giovinetto and Schwertdfeger, 1966). Furthermore, Thompson found no significant trends in accumulation over the 911 a. No evidence exists for a major change in accumulation at Dome C during the last 700 years, either (Lorius and others, 1979).

Bolzan (private communication, 1980) measured borehole temperatures at South Pole and at Dome C. Although a slight warming of perhaps 0.3°C may be indicated at both sites, he found no evidence for temperature changes as large as 0.5°C.

The climate at South Pole and at Dome C has been relatively constant, and no support is found in climatic change for the disagreement between Gow's empirical relation and the observed depth-density profiles. Gow's relation is based on data taken from warmer regions with larger accumulation rates. Apparently, this relation does not apply to the extreme conditions of Dome C.

--DENSITY RANGE DATA

Density range, the maximum difference between densities of adjacent layers, was calculated for various depths, as described above. Density range values are listed in Appendix B, table 2, and density range is plotted on a logarithmic scale against depth in figure 4. The line in figure 4 was fitted using a least-squares regression, and indicates a surface density range of 0.102 Mg m^{-3}, decreasing to 0.0056 Mg m^{-3} at 50 m depth.

Gow (1968) reports a similar rapid decrease in density range with depth for the Byrd Station core, and a surface range of 0.11 Mg m^{-3}. However, he did not specifically sample for density range, so the data are not easily compared.

--DISCUSSION OF DENSITY RANGES

Thin-section studies (described below) and density measurements showed that fine-grained firn is more dense than coarse-grained firn at the same depth. Density ranges are observed to decrease smoothly with depth. It follows that fine-grained firn increases in density more slowly with depth than does coarse-grained firn at the same depth. Furthermore, fine-grained firn increases in density more slowly with depth and with time than does coarse-grained

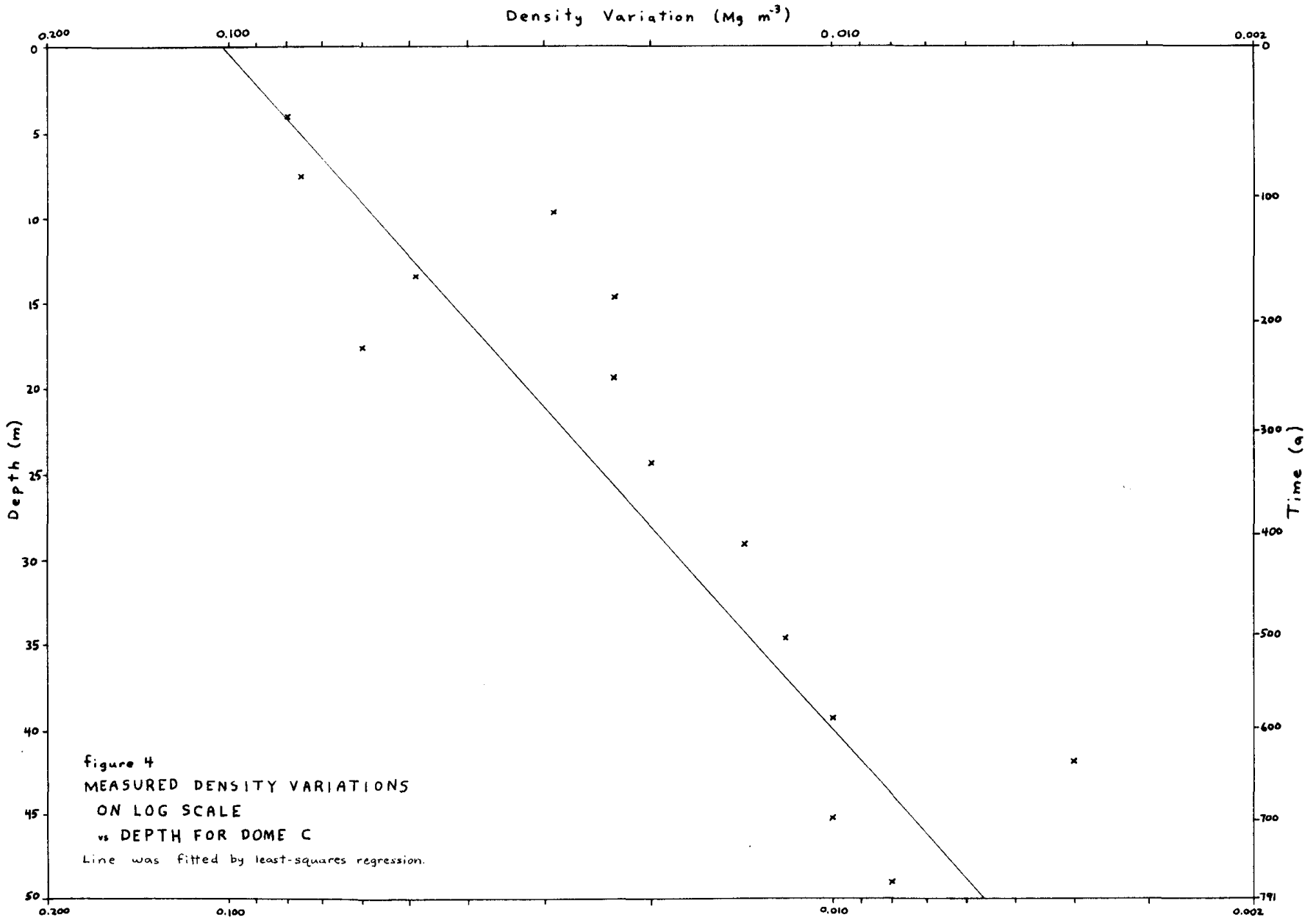

Figure 4
MEASURED DENSITY VARIATIONS
ON LOG SCALE
vs DEPTH FOR DOME C
Line was fitted by least-squares regression.

firn of the same density, although the difference in time-rate of densification between coarse and fine firn of equal density is small.

This raises an interesting problem. Densification of firn has been compared to sintering of ceramics (Gow, 1968 and 1974). For sintering under zero confining stress, the driving force is provided by the free surface energy of a material. In a typical case in ceramics, an increase in particle size from 1 to 10 microns decreases this energy, and the rate of sintering, by a factor of 10. In general, coarse-grained materials should densify more slowly than fine-grained (Budworth, 1970).

It thus becomes important to know why the opposite behavior is observed at Dome C. No plausible mechanism for mass transport out of the fine-grained layers in the isothermal region has been suggested, so the explanation must lie in the rate of sintering.

The fine-grained layers are already relatively dense near the surface, and spread the load over many crystal-crystal bonds representing a large total area. The coarse-grained layers begin with a less-dense structure, with fewer crystal-crystal contacts and less total area of contact (see discussion of specific areas, below). Fine-grained layers average about 50% more bond area than

coarse-grained layers at the same depth, and in general the difference decreases with depth. The difference in rate of densification with depth between coarse and fine firn also decreases with depth. Fine-grained layers have greater crystal-crystal bond area than coarse firn of equal density, although this difference is smaller than that between coarse and fine firn at the same depth.

Relative to fine firn, coarse firn tends to densify more slowly because of less free surface energy, and more rapidly because of less resistance to deformation under load. The observed rates of densification of coarse firn relative to fine firn are apparently controlled by the load factor. For firn at the same depth, the significantly greater crystal bond area of fine firn leads to much slower densification with depth than for coarse firn. For firn of the same density, coarse firn has less crystal bond area and so less resistance to deformation under load than fine firn, but it is subjected to greater load than the fine firn. Thus, similar rates of densification with time are observed.

--LOAD-DEPENDENCE OF DENSIFICATION RATES

Gow (1974) plotted density of firn against the logarithm of its age for the isothermal region (deeper than 10 m) for numerous locations in Greenland and Antarctica.

He found a family of parallel straight lines with intercepts dependent on mean annual temperature. These results are consistent with log-linear densification predicted by Coble (1961a and 1961b) for the sintering of powder compacts. Figure 5 shows the density versus log of age profile for Dome C, and a linear approximation of this profile. The other line in the figure, labelled "unconfined sintering", will be discussed below. As a first approximation, the observed curve is linear in the isothermal region. However, it is clear that from the surface to about 0.575 Mg m^{-3} (well into the isothermal region) densification proceeds slower than the linear approximation, while for densities above 0.575 Mg m^{-3} densification is faster than the approximation. A relatively steady increase in the rate of densification against log of age is observed in both the isothermal and temperature gradient regions. Such an increase is consistent with a model in which densification is affected by load, so that it is accelerated by increasing load. Some of the curves in Gow (1974), and particularly the curve for Plateau Station, show similar deviation from linearity. In general, such deviations are most prominent for locations with low accumulation rates and low temperatures.

At depths greater than those studied in this investigation, the rate of densification against the log of age must decrease,

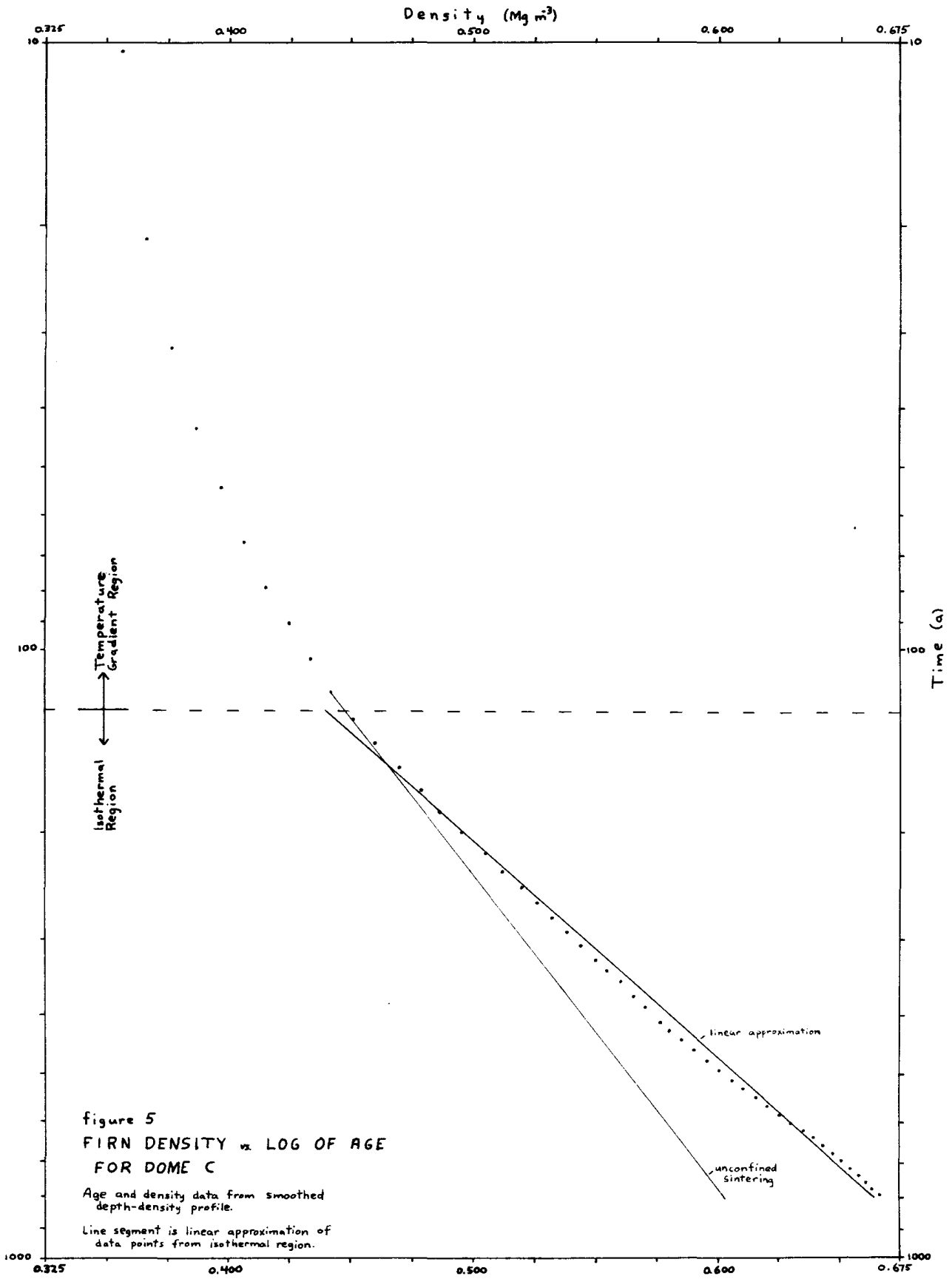

figure 5
FIRN DENSITY vs LOG OF AGE FOR DOME C

Age and density data from smoothed depth-density profile.

Line segment is linear approximation of data points from isothermal region.

as the density asymptotically approaches the density of ice. Instead of being linear, the density-log of age profile is actually a logistic curve.

The work by Coble (1961a and 1961b) dealt with powder compacts. Such compacts are typically compressed to one-half the maximum theoretical density before sintering is begun. Coble found log-linear densification only after an intermediate stage of sintering was attained, characterized by grain growth and significant necking. At 10 m depth at Dome C, the density is still slightly less than one-half the theoretical maximum, but grain growth and necking are well-progressed. Thus, the intermediate stage of sintering appears to begin at about 10 m depth, as Gow suggests.

Firn at 10 m depth at Dome C is already under a load of 39,000 N m^{-2} of firn section. This is, however, only 1/7 of the load at 50 m depth. The tangent to the curve of density against log of age at 10 m (116 a) is an overestimate of the unconfined rate of sintering, but it may not be an extreme overestimate. This curve is shown in figure 5, labelled "unconfined sintering". It is also shown in figure 6, labelled "Dome C unconfined". It is really a maximum value for the rate of unconfined sintering. The difference between this curve and the observed profile plotted in figure 6 is thus an underestimate of the

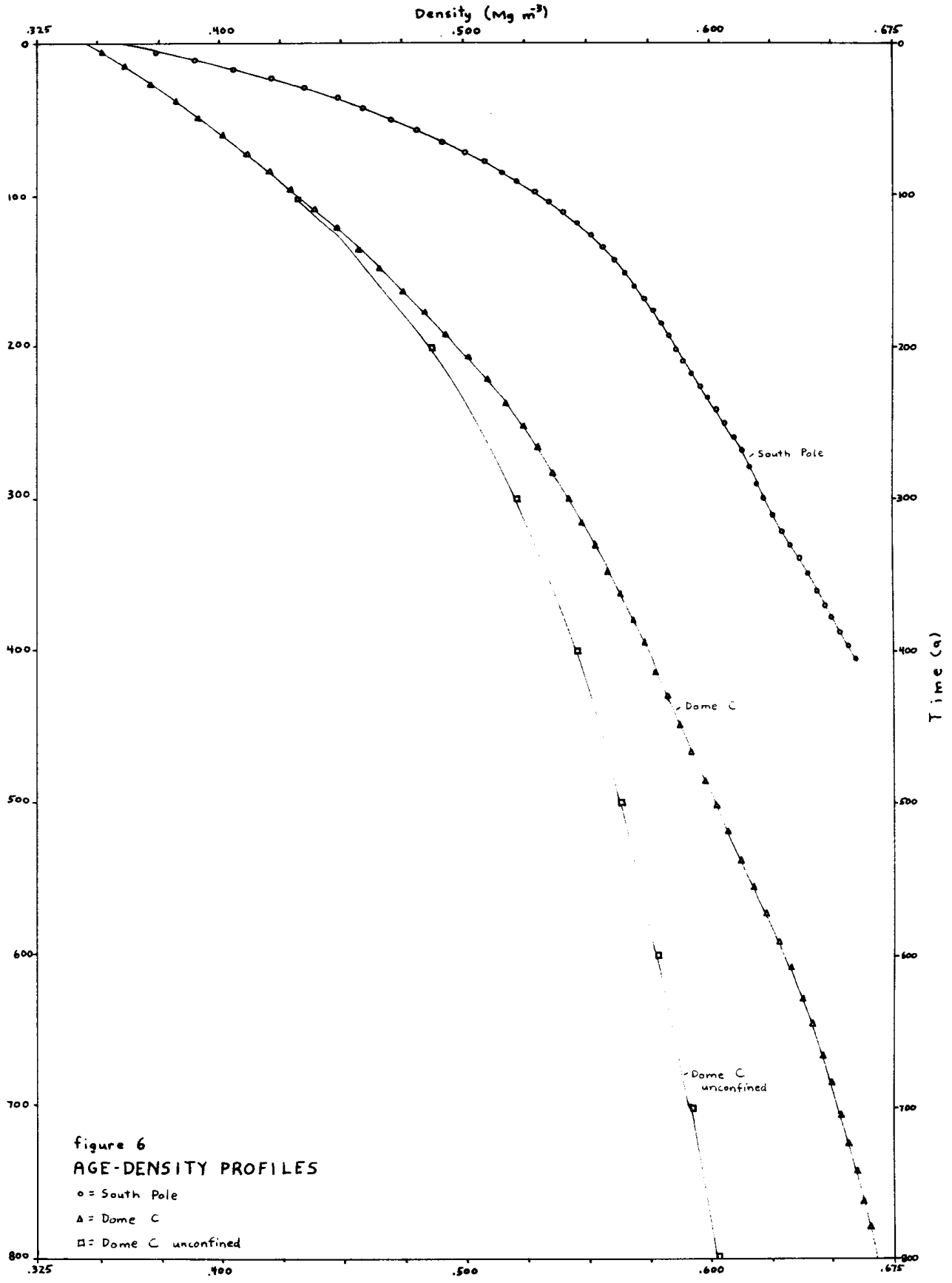

figure 6
AGE-DENSITY PROFILES
o = South Pole
Δ = Dome C
□ = Dome C unconfined

contribution of load to densification. No empirical studies of unconfined sintering rates of Dome C firn at -54.3°C have yet been conducted, to allow evaluation of the accuracy of this estimate.

One other example of the importance of load to densification deserves presentation. The density-age profile for South Pole is plotted in figure 6. Densities are taken from the smoothed curve of Giovinetto's (1960) data, shown in figure 3. 30 year accumulation averages reported by Thompson (1979) were used to calculate ages. Numerical data are presented in Appendix B, table 6.

Near the surface, densities at South Pole are seen to increase more rapidly with time than those at Dome C. This is probably due to the higher mean annual temperature at South Pole. The smaller size of crystals at South Pole (see discussion of crystal areas, below) and other factors, such as mean annual temperature range (Kojima, 1964), may also be important, but temperature seems to be the dominant factor.

Because firn of any given density increases in density more rapidly with depth at South Pole than at Dome C, firn at Dome C is subjected to increasingly greater load than firn of equal density at South Pole.

One would expect that the difference in rates of densification between South Pole and Dome C would decrease with increasing density. This trend does indeed occur, as illustrated by the South Pole:Dome C time-rate of densification ratios in the following table:

DENSITY ($Mg\ m^{-3}$)	RATE OF DENSIFICATION (in 10^{-4} $Mg\ m^{-3}\ a^{-1}$) SOUTH POLE	DOME C	SOUTH POLE: DOME C Ratio	LOAD (in $N\ m^{-2}$) SOUTH POLE	DOME C
0.400	27.7	8.04	3.45	5865	19487
0.450	16.7	6.84	2.44	24596	42494
0.500	14.5	5.77	2.51	46613	68482
0.550	6.08	3.08	1.97	86968	108201
0.600	4.41	2.82	1.56	163051	164591
0.650	3.34	2.10	1.59	255198	229994

Two deviations from the trend are seen to occur. The first is the slight increase in the ratio from 2.44 to 2.51 as density increases from 0.450 to 0.500. It is worth noting that the accumulation rate reported by Thompson (1979) for South Pole for firn near 0.500 $Mg\ m^{-3}$ is the highest rate found in the 911-year record she studied. If the accumulation rate is reduced from her reported value (80.3 $kg\ m^{-2}\ a^{-1}$) to 75 $kg\ m^{-2}\ a^{-1}$, still a very high value, then the ratio for 0.500 $Mg\ m^{-3}$ changes from 2.51 to 2.36, and conforms to the observed trend in ratios.

Below the critical point, firn at South Pole increases in density with depth more slowly than firn at Dome C. For

densities greater than about 0.610 Mg m^{-3}, load at South Pole is greater than load at Dome C. Thus, it is expected that the ratio should increase for densities greater than 0.610 Mg m^{-3}. This is in fact observed.

Thus, the rate of densification at the surface is determined by temperature and other parameters. As load increases, however, it controls how the rate of densification varies.

Densification of firn depends on many factors, including mean annual temperature, crystal size, crystal shape, and crystal bond area (Coble, 1961a and 1961b), and load and annual temperature range (Kojima, 1964) acting over time. The data and discussion presented above indicate that mean annual temperature and load acting over time are the major factors in the 5 to 50 m depth range considered in this study.

CRYSTAL AREA MEASUREMENTS

--METHOD

Thin sections were prepared using a modification of the method described by Bader (1939) and Gow (1969). In this method, pore spaces are filled with an organic liquid, which is frozen to provide strength. Sections of the reinforced firn are prepared on a microtome. Kinosita and Wakahama (1959), Gow (1969), and others favor aniline as a filler. However, it is a highly toxic material which can be dangerous if taken internally, spilled on the skin, or inhaled as a vapor. The threshold concentration for adverse physical effects for an eight-hour exposure is only 0.5 ppm by volume in the air (Allied Chemical Corp., 1964). For small, unventilated cold rooms, those with wooden floors which could absorb spilled aniline and release it into the air over long periods of time, and those where the activities of numerous researchers increase the probability of accidents, aniline presents an unacceptable safety hazard.

The chemical dodecane was selected as a substitute for aniline. Dodecane, $C_{12}H_{26}$, has a well-defined freezing point at -9.6°C, is colorless and transparent when liquid, and is immiscible with water (Weast, 1973). It has very low toxicity; irritation of the eyes by direct

contact, and of the skin by frequent or prolonged contact are the only hazards listed on the U.S. Department of Labor approved Materials Safety Data Sheet (Eastman Kodak Company, 1979). Dodecane is not as strong as aniline when frozen, however, so greater care must be taken to obtain good sections. Where safety is a minor concern, aniline is probably a superior filler. However, when required for safety, dodecane is a good substitute.

Photographs were taken of the prepared thin sections under crossed polaroids, and crystal cross-sectional areas were measured on photographic prints. A modification of the method of Gow (1969) was used. Gow counted the 50 largest grains in an area 17.5 x 12.5 mm, such that he counted about 25% of the grains in each section. This procedure allows for variations in observed grain sizes caused by the position of the plane of section.

For the present study, an area of 30 x 17.5 mm was used. This approximates the useable area of a standard petrographic slide. 50 crystals comprised from 15% to 30% of the crystals on most slides. As in Gow's study, little variation in actual crystal areas in disaggregated firn was observed. However, a few crystals were found which were significantly larger. In thin section, the largest

crystals exceeded the mean cross-sectional area of crystals in their sections by as much as six standard deviations. For this reason, the five largest crystals in each section were eliminated, and the next 50 largest crystals were measured. Apart from neglecting the five largest crystals, the method used here was very similar to that used by Gow.

It is clear that the reported crystal area varies with the percentage of crystals measured in an area and the method by which these crystals are selected. To facilitate comparison, some convention should be adopted which could be used in all studies of high polar firn. A careful consideration of grain size variance and sectioning problems is needed. In the absence of a sounder theoretical basis, the method of Gow (1969) is advocated, but with one minor alteration: the five largest crystals in each section should be eliminated, and the following 50 largest crystals should be measured and averaged.

--RESULTS AND DISCUSSION

Gow (1969) and others have reported that discrete grains composed of more than one crystal can be recognized in the upper 10 m of some sites. At Dome C, virtually all grains observed at 4 m depth and deeper consisted of a single

crystal. Thus, measurements of crystals at Dome C are also measurements of grains. As at other sites, individual grains cannot be recognized below 10 m depth at Dome C, but crystals may still be distinguished in cross-polarized light.

It early became clear that crystal size distinctions associated with the density variations were large enough to complicate any simple trend in crystal areas. Two curves were thus generated; one for fine crystals from dense layers, and one for coarse crystals from less-dense layers. Figure 7 is a plot of crystal cross-sectional area against age. The least-squares linear-regression line for the fine-grained samples was fitted using all of the data points. In the case of the coarse-grained regression line, the shallowest data point was omitted, so that only samples from isothermal depths were considered. This is in accordance with Gow (1969) who found that crystal growth at South Pole was much slower in the isothermal region than in the temperature gradient region. Use or exclusion of the shallowest data point for the fine-grained line makes little difference. Data are recorded in Appendix C, table 1.

Gow (1969) and Stephenson (1967) independently reported that crystal area increases linearly with age;

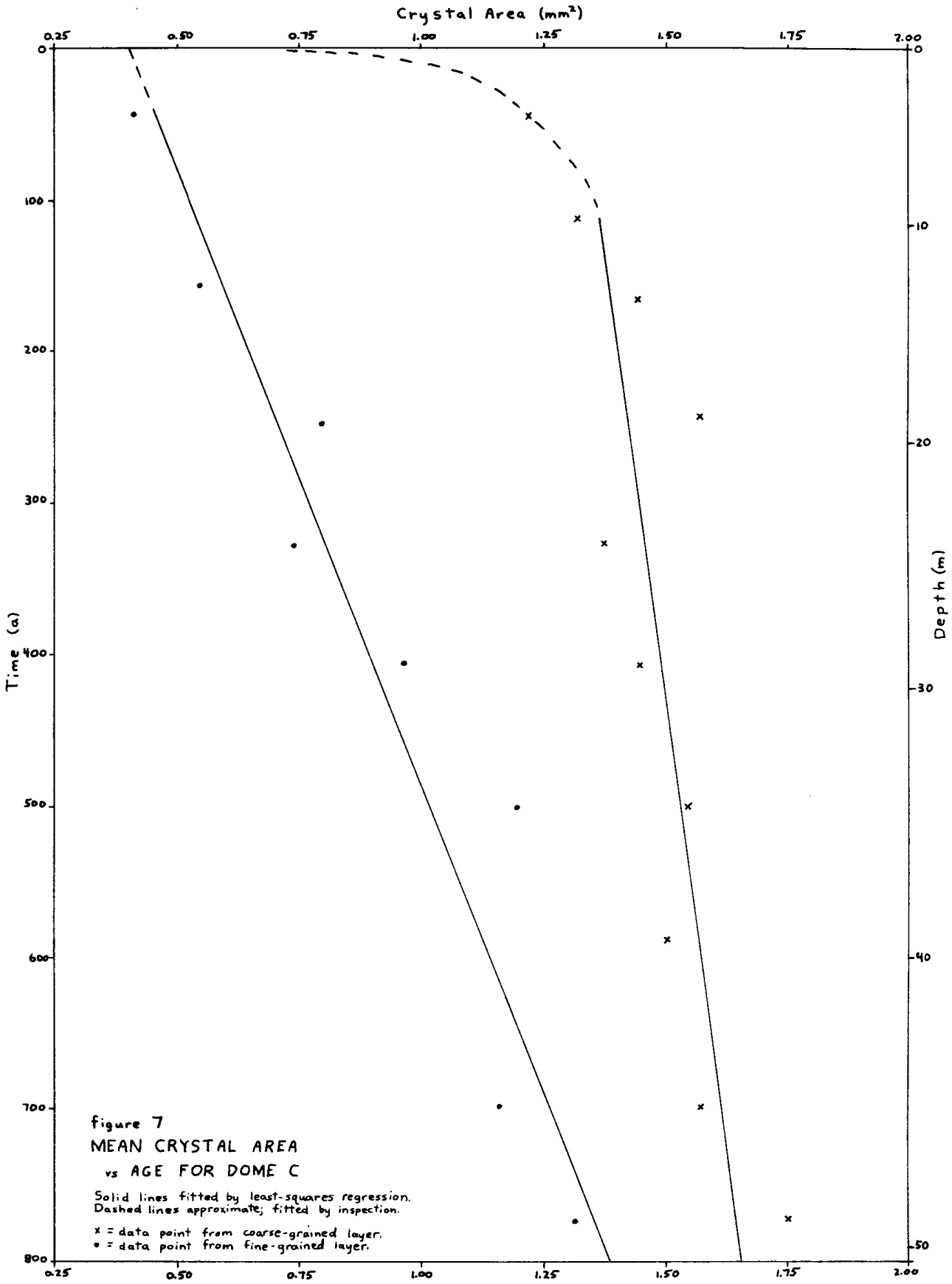

figure 7
MEAN CRYSTAL AREA
vs AGE FOR DOME C

Solid lines fitted by least-squares regression.
Dashed lines approximate; fitted by inspection.

x = data point from coarse-grained layer.
• = data point from fine-grained layer.

that is:

$$D^2=D_o^2+Kt \qquad (4)$$

where D^2 is the mean cross-sectional area at time t, D_o^2 is the extrapolated mean cross-sectional area at time zero, and K is the crystal growth rate, usually expressed in $mm^2\ a^{-1}$.

The Dome C data seem to support this relation well. The coarse-grained line gives a growth rate of about $4.2 \times 10^{-4}\ mm^2\ a^{-1}$. This agrees well with data from Duval and Lorius (in press) for firn from 60 to 360 m depth at Dome C, which gave a growth rate of $4 \times 10^{-4}\ mm^2\ a^{-1}$. Extrapolated to 50 m depth, the curve from Duval and Lorius gives a crystal area of $1.3\ mm^2$. This agrees well with the data in figure 7, if it is remembered that figure 7 shows the coarsest firn rather than the average, and that Duval and Lorius used a slightly different method for measuring crystal sizes which will lead to slightly smaller reported values. The fine-grained growth rate is about $1.2 \times 10^{-3}\ mm^2\ a^{-1}$, almost three times the rate for coarse firn.

Gow (1969) related rate of crystal growth to age by the equation

$$K=K_o \exp(-E/RT) \qquad (5)$$

where K is the crystal growth rate as defined above, K_o is a constant, R is the gas constant, T is the isothermal firn temperature in degrees Kelvin, and E is the activation energy of the growth process.

Based on observed growth rates and temperatures for a large number of sites, Gow determined an activation energy of 44.5×10^3 J mole^{-1}. Extrapolating his relationship to -54.3°C one obtains a crystal growth rate of 4.1×10^{-4} mm^2 a^{-1}, which agrees with the values reported from this study and from Duval and Lorius. This helps confirm Gow's findings, and also lends support to the statement that the coarse crystals at Dome C are not far from the average.

Of some interest is the much higher growth rate for fine firn relative to coarse firn at the same temperature. Based on one data point, it is not possible to determine the activation energy for fine firn. If K_o should be the same for fine and coarse firn, then fine firn would have an activation energy roughly 2000 J mole^{-1} less than coarse. Data from other locations are required to test this.

At South Pole, Gow (1969) found crystals averaging only 0.65 mm^2 at 50 m depth. Crystals at Dome C average

over 1.0 mm^2 at only 10 m depth, where they are both shallower and younger than the 0.65 mm^2 crystals at South Pole.

Two major factors contribute to the larger crystals at Dome C. First, Gow (1969) observed that crystals at South Pole grow rapidly in near-surface regions. He attributed the large observed growth rate to temperature gradients in combination with the long time spent by the firn under the influence of the gradients. He reported that crystals increased from 0.18 mm^2 at an age of one year (0.1 m depth) to 0.43 mm^2 at 62 years (10 m depth), with most of the increase in the first 20 years (4 m). 10 m depth is the approximate limit of temperature gradients. This is a rate of increase of 4.1×10^{-3} mm^2 a^{-1} in the nonisothermal region, nearly an order of magnitude larger than the South Polar isothermal growth rate of 6.0×10^{-4} mm^2 a^{-1}. At Dome C, coarse firn at 10 m depth is 117 years old and has a mean cross-sectional crystal area of about 1.35 mm^2. If the growth rate in the upper 10 m at Dome C is the same as for South Pole, then crystals at 0.1 m depth would be about 0.87 mm^2; significantly smaller than at 10 m depth, but still larger than crystals at South Pole.

However, Dome C is at a lower latitude than South Pole, and receives more intense insolation. This leads to very rapid recrystallization in very shallow firn. Observations at Dome C by Ron Coffman (private communication, 1980) indicate that much of the recrystallization is accomplished in the upper 0.1 m, so that crystals are indeed approaching 1 mm^2 by the time they reach that depth.

At Vostok Station, with a mean annual temperature of -56.6°C (Korotkevitch and others, 1978) and a mean annual accumulation of 22 kg m^{-2} a^{-1} (Barkov and others, 1974) crystals average about 1.0 mm^2 near the surface (Korotkevitch and others, 1978). It is possible that, due to the small amount of insolation received and relatively large accumulation rate, South Pole will prove to have some of the smallest crystals in polar firn anywhere.

SPHERICITY MEASUREMENTS

--METHOD

It is possible to learn something of the shape of a crystal by measuring the diameter of the largest inscribed circle and the smallest circumscribed circle that can be constructed for a cross-section of that crystal. These diameters were measured for the 55 largest crystals in each thin section, and the mean values for inscribed circles (M_i) and circumscribed circles (M_c) were calculated. From these sphericity ($S=M_i/M_c$), Riley sphericity (S^2) (Folk, 1974), or mean proportion (1/S) (Narita and others, 1978) can be calculated. The sphericity (S) was chosen to illustrate the processes occurring at Dome C.

--RESULTS AND DISCUSSION

Figure 8 shows M_i, M_c, and S for coarse-grained and fine-grained firn plotted against depth. Numerical data appear in Appendix C, table 2.

It should be remembered that sphericity estimates a three-dimensional property, but that all of the measurements reported here were made in the horizontal plane, thus introducing a possible bias. A few sections cut in the vertical plane revealed no significant preferred orientation below about 10 m depth. In shallower layers, however, such a preferred orientation was observed (see Appendix D, section I).

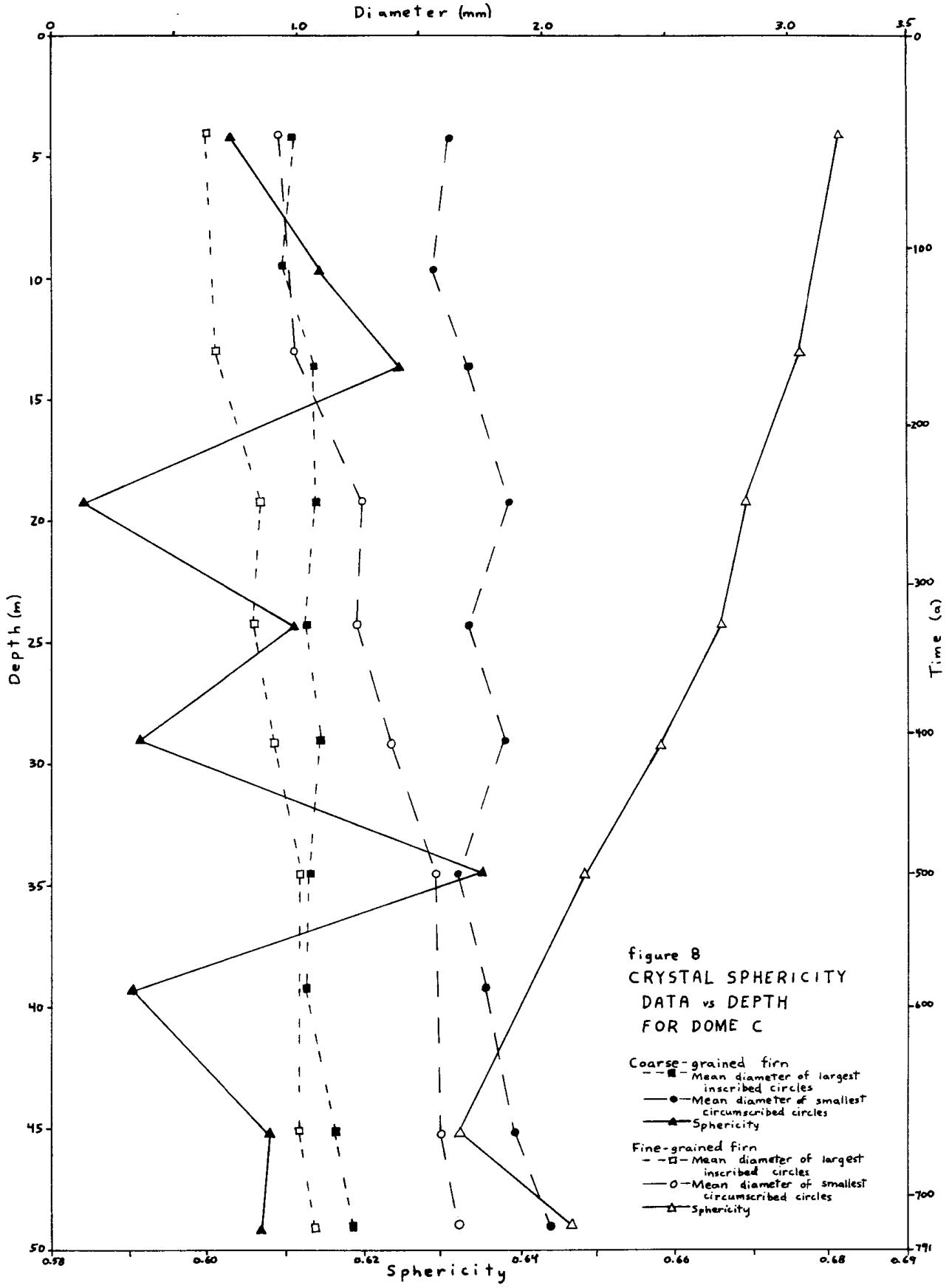
Diameter (mm)
0
1.0
2.0
3.0
3.5
Depth (m)
5
10
15
20
25
30
35
40
45
50
Time (a)
100
200
300
400
500
600
700
791
0.58
0.60
0.62
0.64
0.66
0.68
0.69
Sphericity
figure 8
CRYSTAL SPHERICITY DATA vs DEPTH FOR DOME C
Coarse-grained firn
Mean diameter of largest inscribed circles
Mean diameter of smallest circumscribed circles
Sphericity
Fine-grained firn
Mean diameter of largest inscribed circles
Mean diameter of smallest circumscribed circles
Sphericity

Spherical grains have a sphericity of 1. More-or-less regular polyhedra with many sides have relatively high sphericities. Strongly-elongate or highly-irregular objects have low sphericities, approaching zero in the limiting case. Freshly-fallen snow recrystallizes rapidly to more nearly spherical grains (LaChapelle, 1969). Thereafter, necking occurs between grains. Eventually, the necks between grains widen, the spaces between necks are filled in, and polyhedra form. Thus, one might expect to find sphericities decreasing from the surface (isolated grains) to some point (maximum necking) and then increasing again (filling in between necks).

The fine-grained firn appears to demonstrate this expected trend well. Sphericities are high near the surface, decrease steadily with depth through 45 m, and then increase. The decrease is well-defined, although the increase near 50 m depth is based on one point and might be open to dispute.

The coarse-grained curve reveals no such simple relation. Extensive recrystallization occurs near the surface in coarse layers, so that prominent necks are observed to exist by 4 m depth. The sphericity is thus quite low there. Thereafter, much variability is observed in the sphericity curve, but no general trend.

According to Palais (1980) the coarse firn really consists of depth hoar, soft snow, and intermediate snow. Apparently, the large scatter of data points is due to the different types of firn included under the label "coarse". Coarse firn recrystallizes slowly, so that any general trend that might exist is masked under the variability.

It is possible that careful study would allow the distinction of different types of coarse firn at depth, based on sphericity plus grain size and other characteristics, but such identification is beyond the scope of the present investigation.

SURFACE AREA MEASUREMENTS

--METHOD

Based on probability theory, Smith and Guttman (1953) developed a method to estimate specific areas of crystal boundary (ice-ice interface) and internal free surface (ice-air interface). For a random surface in any three-dimensional system:

$$S=2N/L \qquad (6)$$

where S is the specific area in $m^2\ m^{-3}$, L is the total length of lines drawn with an arbitrary spacing on the surface in meters, and N is the number of intersections between the lines and the surfaces as seen on the plane of section.

Approximately 0.3 m of total line was used on each section, yielding about 400 or more total (ice-ice + ice-air) intersections. This method is similar to that described by Narita and others (1978).

--RESULTS AND DISCUSSION

The results are displayed in figure 9, and are listed in Appendix C, table 3. The rapid growth of fine crystals is reflected in the sharp decrease in internal free surface of the fine layers with depth. Slower growth of coarse

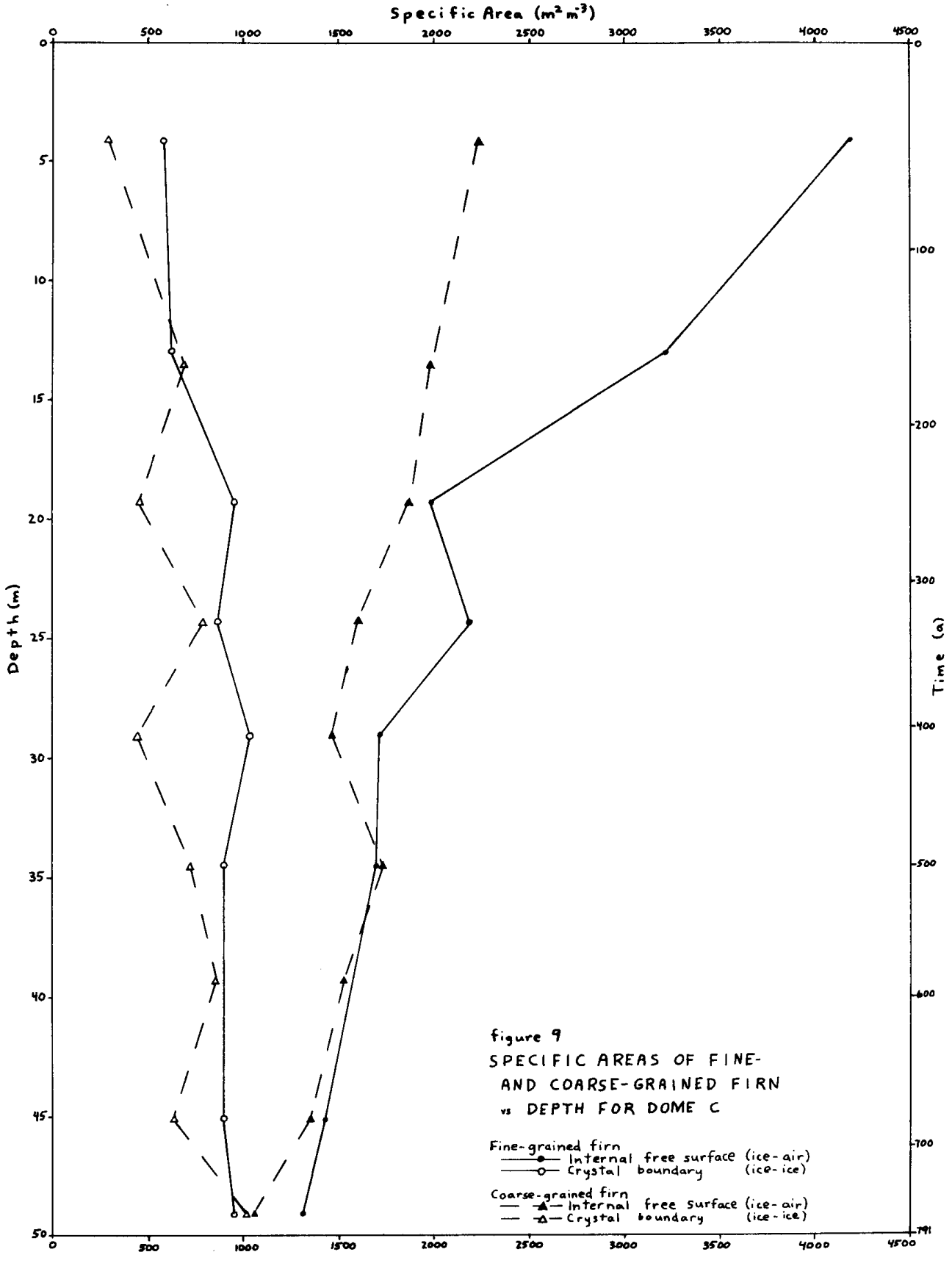

figure 9
SPECIFIC AREAS OF FINE- AND COARSE-GRAINED FIRN vs DEPTH FOR DOME C

crystals is also shown in the slower decrease in free surface for the coarse layers.

As expected, fine layers show greater internal free surface and crystal boundary than corresponding coarse layers. If crystal growth is indeed due to the interfacial free energy of the grain boundaries (Burke and Turnbull, 1952; Gow, 1974) then the greater surface areas in fine-grained firn would help explain the greater rate of crystal growth.

Crystal boundary surface area increases more slowly than internal free surface decreases for both coarse and fine firn, because crystal growth partly offsets the effects of increased crystal bond area.

SUMMARY AND CONCLUSIONS

Firn at Dome C is deposited in distinct layers which are easily distinguished to a depth of 50 m. These layers consist of several types of firn, but this study is concerned with just two layer types: fine-grained dense layers that comprise a small amount of the core, and coarse-grained, low-density layers that comprise most of the core. The dense layers are probably late-summer wind crusts, while the coarse layers include firn formed during fall, winter, and spring.

Density increases with depth, and exhibits the critical point at about 0.51 Mg m^{-3}, as predicted by Benson. However, the change in densification rate with depth at the critical point is smaller for Dome C than for most other locations.

Significant differences exist between the depth-density profiles of Dome C and South Pole, indicating that the empirical relation discovered by Gow relating depth-density profiles of sites with different mean annual temperatures and accumulation rates may not apply to locations with lower temperatures and accumulation rates than South Pole.

Fine-grained firn is observed to increase in density more slowly than coarse-grained firn, in violation of the predictions of a simple sintering model for densification

based on free surface energy. Fine-grained firn has greater crystal-crystal bond area than coarse-grained firn, and so greater resistance to deformation under load. This indicates that deformation under load is more important than free surface energy in determining the relative rates of densification of coarse and fine firn, and that deformation under load is a primary mode of densification.

The deviations of the Dome C age-density profile from that for South Pole, and of the Dome C density profile from log-linear densification with time reveal similar information about the densification of firn. Low temperature and load cause slow densification, while higher temperature and load speed densification. Load and temperature acting over time seem to be the most important factors in densification.

Thin sections of firn are often prepared using aniline as a filler. However, aniline is a highly toxic chemical. Where safety is a major concern, dodecane is a suitable substitute for aniline.

Crystal growth rates for coarse layers agree well with the value predicted by Gow based on empirical studies of other locations. However, crystal sizes at Dome C are much larger than expected. This may be due to the low latitude of Dome C, leading to intense insolation and much recrystallization in the upper 0.1 m. Long residence time

in the region of temperature gradients due to low accumulation may also be important.

Fine crystals exhibit much higher growth rates than crystals in coarse layers, and also have greater internal free surface and internal grain boundary. This supports the hypothesis that recrystallization is driven by crystal free surface energy.

A steady decrease in crystal sphericities in fine layers from 5 to 45 m depth shows progressive necking between grains which were more nearly spherical near the surface, while a reversal of this trend below 45 m depth is due to filling in between necks. Great variation in sphericities in coarse layers with depth is due to the genetically different types of firn classified as coarse, and effectively masks any trend in sphericity with depth.

More work is required to distinguish the different types of coarse firn. A standard method for measuring crystal sizes which can be used on all polar glaciers is desirable. Growth rates for crystals in crusts should be measured at other locations to allow the calculation of the activation energy for crystal growth in fine-grained firn. Densification rates should also be measured for fine-grained firn for other locations, as such data may help determine the relative importance of load to the densification of firn.

REFERENCES

Allied Chemical Corp. 1964. Aniline. New York, 109 p.

Bader, H. and others. 1939. Der Schnee und seine Metamorphose. Beiträge zur Geologie der Schweiz. Geotechnische Serie. Hydrologie, Lief. 3. (English translation: U.S. Snow, Ice, and Permafrost Research Establishment Translation 14, 1954.)

Barkov, N.I. and others. 1974. The first results of the study of ice cores from the borehole at Vostok Station, Antarctica with the oxygen isotope method. DOKLADY of the Academy of Sciences of the USSR, vol. 214, no. 6, p. 1383-86.

Benson, C.S. 1962. Stratigraphic studies in the snow and firn of the Greenland ice sheet. U.S. Snow, Ice and Permafrost Research Establishment Research Report 70.

Brooks, B.T. and others, ed. 1954. The Chemistry of Petroleum Hydrocarbons, vol. 1. New York, Reinhold Publishing, 664 p.

Budworth, D.W. 1970. An Introduction to Ceramic Science. Oxford, Pergamon Press, 287 p.

Burke, J.E. and Turnbull, D. 1952. Recrystallization and grain growth. Progress in Metal Physics, vol. 3, p. 220-92.

Chang, T.C. and others. 1976. Microwave emission from snow and glacier ice. Journal of Glaciology, vol. 16, no. 74, p. 23-39.

Coble, R.L. 1961a. Sintering crystalline solids, I. Intermediate and final state diffusion models. Journal of Applied Physics, vol. 32, no. 5, p. 787-92.

Coble, R.L. 1961b. Sintering crystalline solids, II. Experimental test of diffusion models in powder compacts. Journal of Applied Physics, vol. 32, No. 5, p. 793-99.

Duval, P. and Lorius, C. In press. Crystal size and climatic record down to the last ice age from Antarctic ice. Earth and Planetary Science Letters.

Eastman Kodak Company. 1979. Dodecane Material Safety Data Sheet. Rachester, New York.

Folk, Robert L. 1974. Petrology of Sedimentary Rocks. Austin, Texas. Hemphill Publishing, 182 p.

Giovinetto, M.B. 1960. Glaciology report for 1958, South Pole station. Ohio State University Research Foundation Report 825-2-Part IV.

Giovinetto, M.B. and Schwertdfeger, W. 1966. Analysis of a 200-year snow accumulation series from the South Pole. Archiv fllr Meteorologie, Geophysik, und Bioclimatologie, series A, Band 15, Heft 2, p. 227-50.

Gow, A.J. 1968. Deep core studies of the accumulation and densification of snow at Byrd Station and Little America V, Antarctica. U.S. Army Cold Regions Research and Engineering Laboratory Research Report 197.

Gow, A.J. 1969. On the rates of growth of grains and crystals in South Polar firn. Journal of Glaciology, vol. 8, no. 53, p. 241-52.

Gow, A.J. 1974. Time-temperature dependence of sintering in perennial isothermal snowpacks (in Snow Mechanics Symposium: Proceedings of the Grindelwald Symposium, April, 1974. IAHS-AISH Publication no. 114, p. 25-41.)

Kinosita, S. and Wakahama, G. 1959. Thin sections of deposited snow made by use of aniline. Teion-kagaku: Low Temperature Science, ser. A, no. 18, p. 35-45.

Koerner, R.M. and Kane, H.S. 1967. Glaciological studies at Plateau Station. Antarctic Journal of the United States, vol. 2, no. 4, p. 122-23.

Kojima, Kenji. 1964. Densification of snow in Antarctica (in Mellor, Malcom, ed. Antarctic Snow and Ice Studies, Antarctic Research Series, vol. 2, American Geophysical Union Publication no. 1197. Washington, D.C., p. 157-218.)

Korotkevitch, E.S. and others. 1978. Results of the study of the vertical structure of the Antarctic ice sheet in the vicinity of Vostok Station. Bulletin of the Soviet Antarctic Expedition 97, p. 135-48.

LaChapelle, Edward R. 1969. Field Guide to Snow Crystals. Seattle, Washington. University of Washington Press, 101 p.

Langway, C.E. 1958. Ice fabrics and the universal stage. U.S. Army Snow, Ice and Permafrost Research Establishment Technical Report 62.

Lax, J.N. 1978. A physical model for thermal conductivity of low-temperature snow (M.Sc. thesis, Ohio State University, unpublished.)

Lorius, C. and others. 1979. 30,000 year isotope climatic record from Antarctic ice. Nature, vol. 280, no. 5724, p. 644-48.

Narita, Hideki and others. 1978. Structural characteristics of firn and ice cores drilled at Mizuho Station, East Antarctica (In Kusunoki, Kou and Suzuki, Yosio, ed. Ice coring project at Mizuho Station, East Antarctica, 1970-1975. Memoirs of National Institute of Polar Research, Special Issue no. 10, p.48-51.)

Palais, Julie. 1980. (M. Sc. thesis, Ohio State University, unpublished.)

Paulcke, W. 1934. Der schnee und seine Diagenese. Zeitschrift für Gletscherkunde, vol. 21, no. 4, p. 259-82.

Raynaud, D. 1976. Les inclusions gazeuses dans la glace de glacier; leur utilisation comme indicatuer du site de formation de la glace polaire; applications climatiques et rheologiques (These de Doctorat d'etat, Universite Scientifique et Medicale de Grenoble, unpublished.)

Raynaud, D. and others. In press. Crystal size and total gas content of ice: two indicators of the climatic evolution of polar ice sheets (in Proceedings of the International Conference of Planetary Atmospheres and Climatology of the Earth, Nice, 16-20 October, 1978.)

Smith, C.S. and Guttman, L. 1953. Measurement of internal boundaries in three-dimensional structures by random sectioning. Journal of Metals, vol. 5, no. 1, p. 81-7.

Stephenson, P.J. 1967. Some considerations of snow metamorphism in the Antarctic ice sheet in the light of ice crystal studies (In Ōura, H., ed. Physics of Snow and Ice: International Conference on Low Temperature Science...1966...Proceedings, vol. 1, Pt. 2 (Sapporo), Institute of Low Temperature Science, Hokkaido University, p. 725-40.)

Thompson, Ellen Mosley. 1979. 911 years of microparticle deposition at the South Pole: A climatic interpretation. (Ph. D. thesis, Ohio State University, unpublished.)

Tongiori, E. and others. 1962. Deep drilling at Base Roi Baudouin, Dronning Maud Land, Antarctica. Journal of Glaciology, vol. 4, no. 31, p. 101-10.

Weast, Robert C., ed. 1973. Handbook of Chemistry and Physics, 54th edition. Cleveland, Ohio. Chemical Rubber Company.

Zwally, H. Jay. 1977. Microwave emissivity and accumulation rate of polar firn. Journal of Glaciology, vol. 18, no. 79, p. 195-215.

APPENDIX A--METHODS USED

--DENSITY MEASUREMENTS

It was decided to calculate the density of each sample from measurements of length, cross-sectional area, and mass. The samples were in the form of right cylinders, and were thus easily measured. The large permeability of the samples precluded the use of immersion or floatation techniques.

Samples were cut from the core using a standard bandsaw with mitre guide and rip fence. Typical samples ranged from 15 mm to 25 mm in thickness. Irregular surfaces or non-parallel cuts were rectified by shifting the rip fence a millimeter or two closer to the blade and carefully surfacing the sample.

After cutting, loose ice shavings were brushed from the sample. Care was taken to avoid any disruption of the structure. On samples from shallow depths, loose grains had recrystallized onto the outside of the core during storage. These were removed by brushing or by cutting with a pocket knife.

Dimensions were measured with a sliding micrometer calibrated in millimeters, and were estimated to the nearest 0.1 mm. In cases where the ends of a sample were not parallel, several thickness measurements were taken around the perimeter of the sample, and an average value was recorded. The core sections often deviated slightly from round, so many diameters were measured and an average was recorded. Tests indicate

that thickness measurements are reproducible to about 0.1 mm. Diameter measurements are reproducible to 0.4 mm for samples from shallow depths, but reproducibility improves with depth.

Mass measurements were made on a triple-beam balance calibrated to 0.01 g, and were recorded to the nearest 0.01 g. Even allowing for errors in cleaning recrystallized and powdered ice from the samples, the reproducibility is easily 0.05 g.

A typical sample would thus be 20.0 mm $\pm$ 0.5% thick, 75.0 mm $\pm$ 0.4% in diameter, and 50.00 g $\pm$ 0.1% in mass. This gives a calculated density of 0.566 Mg m^{-3} $\pm$ 1.0%.

Density measurements were also made for entire 1 m core sections. Length was determined with a meter stick, reproducible to 2 mm. Diameter was measured at three evenly-spaced locations along the core in two mutually-perpendicular directions with a large screw micrometer, and an average was computed. Diameter is reproducible to 0.4 mm. Mass was measured on a triple-beam balance with added balance weights, and is reproducible to about 2 g. A typical sample would be 990 mm $\pm$ 0.2% long, 75.0 mm $\pm$ 0.5% in diameter, and 2500 g $\pm$ 0.08% in mass, for a calculated density of 0.572 Mg m^{-3} $\pm$ 0.8%.

For core sections less than 2611 g total, it was possible to determine the mass in one measurement. For heavier cores, it was necessary to cut or break the core and make two

successive mass determinations. This may have introduced slight error. The mistake was made of measuring full meter densities after smaller samples had been cut from some core sections. This, too, could introduce error. Finally, ice recrystallized on the core sections seriously complicated the procedure. Removal of this was a tedious, inexact task accomplished by vigorously rubbing the outside of a core section with a gloved hand.

Ideally, density measurements for full 1 m core sections should be made at the drill site, or as soon as possible thereafter, before the core has time to recrystallize, break, or be otherwise altered.

--THIN-SECTIONING TECHNIQUE

Thin sections were cut from the samples taken to study density ranges. Standard petrographic slides (27 mm x 46 mm) were used. For better adhesion, all slides were roughened on one side on a 400 grit lap.

Initially, it was intended to prepare sections using the method of Gow (1969). In this method, firn to be sectioned is saturated with the organic chemical aniline and then frozen. The aniline strengthens the firn so that its structure is unaltered during sectioning. Aniline, however, is a very toxic chemical. It is readily absorbed through the skin in dangerous amounts, and may be harmful or

fatal if swallowed or inhaled. Eight hour exposure to 0.5 ppm vapor in the air by volume is the threshold for harmful effects. Aniline should be stored and used only in a fume hood (Allied Chemical Corp., 1964).

Dr. Gow works in a large cold room, which is reserved for his use and provided with external ventilation (Gow, private communication, 1979). Thus, by observing rigorous safety procedures, he can safely use aniline. However, the Ohio State University Institute of Polar Studies (IPS) cold room is somewhat smaller than the one used by Dr. Gow, is used consistently by several researchers, and may be provided with external ventilation only by opening the main door. It has a wooden floor, which would quickly absorb any spilled aniline and release it slowly to the air. Also, it is probable that students in the future will conduct thin-sectioning experiments. During the time when each new researcher is learning the technique, there is much greater opportunity for accident. For these reasons, aniline was judged to be too hazardous to use.

A substitute liquid was then required with the following properties: melting point well-defined between $-5^{\circ}C$ and $-15^{\circ}C$; transparent; colorless; low viscosity; high strength when frozen; immiscible with water; low toxicity; low to moderate cost; easy availability.

The chemical finally selected is dodecane. Dodecane, $C_{12}H_{26}$, is the twelfth alkane. It has a molecular weight

of 170.34, a density of 0.7487 Mg m^{-3} at 20°C, a boiling point of 216.3°C at one atmosphere, a freezing point of -9.6°C, and is immiscible with water (Weast, 1973). It exhibits low viscosity right down to the freezing point, and the freezing point is well-defined. It is a colorless liquid with a faint odor and negligible vapor pressure at room temperature and below. It is considered stable unless in the presence of strong oxidizers, and will not undergo hazardous polymerization. Contact with the eyes may cause irritation; treatment involves flushing with water for 15 minutes, and then getting medical attention. Prolonged or repeated contact with the skin may cause irritation; in case of skin contact, the area should be flushed with water. Thermal decomposition or burning generate only CO_2 and CO (Eastman Kodak Company, 1979). In the galaxy of modern chemicals, dodecane is one of the safest available.

Disadvantages of dodecane include its relative softness, triclinic habit, and whitish translucence when frozen. Where safety is not a major concern, aniline is probably a superior chemical. However, for the IPS cold room and other places where safety is a problem, dodecane is clearly superior.

To prepare a thin section, a rectangle of firn roughly 25 mm x 40 mm and 10 mm thick is cut from a density sample using a bandsaw. This firn is placed on a roughened slide. Chilled dodecane is applied with an eyedropper, saturating

the firn. The IPS cold workroom is typically -12°C, so the dodecane freezes in about a minute. More dodecane is then applied. This is continued until all pore spaces are filled with frozen dodecane and surplus liquid begins to run off rather than soak in (usually a total of four applications).

Although dodecane is almost wholly immiscible with water, it is still advisable to water saturate all dodecane before use. This is easily accomplished by dropping a few ice crystals from one of the core sections into liquid dodecane and waiting a few days, stirring occasionally.

Once the sample is thoroughly saturated with dodecane and frozen onto the slide, it is split on the bandsaw, leaving about 3 mm of firn on the slide. Although this cut occasionally causes a small amount of plucking, it usually leaves a clean, unaltered surface. The saturated firn cut from the slide should be saved. If any error is made in preparing the first thin section, it can be used for a second attempt. If not, it can be melted down and the dodecane recycled.

A second microscope slide is now obtained, and identification numbers are scratched on the smooth side with a diamond scriber. The saturated firn with slide attached is placed on the roughened surface of this second slide. By breathing very lightly on the first slide, the dodecane

may be melted and the slide removed without altering the firn. More dodecane is then added, and the sample is allowed to freeze solidly to the second slide.

The upper surface of the sample was originally cut on the bandsaw without dodecane for support, and is thus subject to significant plucking. However, the plucking can only extend about one grain deep, and the sample is approximately three grains deep at this point. The lower surface, in contact with the second slide, was cut through dodecane and is not subject to plucking. Thus, by removing the upper surface of the sample, an unaltered, unplucked section can be obtained.

To accomplish this, the slide is placed on the stage of a microtome. Distilled water (or water obtained by melting firn), chilled almost to freezing is applied around the slide with an eyedropper, freezing the slide to the stage. The microtome is then used to surface the sample.

The ideal thickness of each microtome cut is controlled by such factors as knife angle and sharpness, and sample density and structure. As a general rule, 25 microns may be removed with each stroke at the beginning, and only 5-10 microns as the final thickness is approached. The sample should be monitored carefully during sectioning. At any sign of plucking, fractures, or other strain, two actions should be taken. First, to fill any holes or

fractures, a thin layer of dodecane should be applied and allowed to freeze. Second, the thickness of each cut should be reduced.

According to Gow (1969) the sample should be reduced to a thickness of one-half the average grain diameter. In practice, this ideal is difficult to achieve. The method adopted to approximate this is serviceable if not exact; it is accurate enough for studies such as this. On any thick section, grain boundaries may be observed in deeper layers by looking through crystals on the top of the section. As the sample is thinned, progressively fewer boundaries may be seen through crystals. When the sample appears to consist of a single layer of crystals, it is almost thin enough.

Once the proper thickness is achieved, the slide is pried from the microtome stage with a pocket knife. If care is exercised, the slide may be removed with little danger of breakage. A cover slip may then be placed on the sample. The slide should be stored in a closed container with some ice chips, so that the air is saturated and sublimation from the sample is minimized.

At every step in this procedure, care should be taken to avoid spilling dodecane, and all dodecane and dodecane-ice mixtures should be recovered for recycling. Although dodecane is nearly nontoxic, prudence dictates that exposure to any

chemical should be minimized. Also, the total cost of this procedure is reduced by recycling dodecane. Most of the dodecane used may be recovered by fixing a plastic bag under the microtome. The recovered ice and dodecane chips may be placed in a beaker and warmed gently, melting the dodecane so it may be poured off. If the ice also melts, the lower density of the dodecane will cause it to rise to the surface, and it can be decanted.

Examination of thin sections prepared in the manner outlined above has shown that, while some internal fractures may develop in crystals, the network of crystals and necks is undisturbed. Limited plucking may be observed in some slides, but most are clean and unaltered. Dodecane decreases in volume only slightly when it freezes (Brooks and others, 1954). Repeated tests indicate that grains are not pulled inward when the dodecane freezes. The multiple applications of dodecane employed in the sectioning procedure ensure that all pores are thoroughly filled in spite of this contraction.

--PHOTOGRAPHIC TECHNIQUE

For ease of study, it was decided to photograph the prepared thin sections and measure crystal size and other parameters from the photographs.

Two different procedures were used in the course of this study. In the first procedure, photographs were taken

using a Rigsby stage (Langway, 1958) as a convenient stand. A number of slides to be photographed were placed on a glass plate, which was placed directly on the polarizing filter built into the stage. An identification number and scale on a strip of drafting paper were placed on each slide. Three incandescent lights totalling 350 watts were focused through the filter using reflectors and the mirror of the stage. The incandescent lights served both to illuminate the slides and to melt the dodecane. The triclinicity and strong translucence of frozen dodecane require that it be melted before being photographed. A number of ice crystals sandwiched between two slides should be kept among the slides to be photographed. As long as these crystals remain unaltered, it is safe to assume that the samples are not being melted.

A 35 mm single lens reflex camera with an f 3.5 1:1 macro lens was clamped to the vertical arm of the Rigsby stage with a C-clamp tripod. A cable release was used to reduce vibration. All samples on the stage were photographed under plane-polarized light by turning the glass plate to bring each slide in turn under the camera. A polarizing filter was then screwed onto the lens, and adjusted so that its plane of polarization was at right angles to that of the filter in the stage. All samples were then photographed under cross-polarized light.

Because of the low light conditions, ASA 400 film was used for both color and black-and-white photos. Typical settings were 1/125 s at f 5.6 for plane-polarized photos, and 1/60 s at f 3.5 for cross-polarized photos. Commercial 3½" x 5" prints were ordered, and measurements were taken from them.

An improved photographic technique was developed by Ron Coffman of IPS for the latter part of this investigation. A polarizing filter was mounted on a ring stand. A clamp was machined to firmly hold the camera above this filter on the stand. As before, a macro lens with attached polarizing filter adjusted for cross-polarization was used. For easy handling, samples were placed on a large glass plate, which was placed on the lower polarizing filter. A heat lamp was used to melt the dodecane.

Instead of incandescent light, a standard electronic strobe was used, shielded by a piece of tissue paper to diffuse the light. With ASA 64 film and 1/60 s shutter speed, f 16 was found to provide good cross-polarized photos, although picture quality was not seriously altered between f 11 and f 22. Optimum exposures will vary with the strobe and exact apparatus used, so each investigator should test to determine the best settings.

Only cross-polarized, color pictures were taken with this method, because they best displayed all of the

information needed for this investigation. Pictures obtained using this method are consistently sharper and show better color resolution than those taken with the earlier method. Although some improvement is still possible, the new method is a distinct improvement. The slowness of the method is a major drawback; it is even slower than the previous method. Problems were also experienced in the camera-strobe cord-strobe system when it became thoroughly chilled, so that it was necessary to warm the system periodically to make it work.

--SAMPLING PROCEDURE

It was initially decided to sample the core "randomly"; that is, without regard to visible structure in the core. The core arrived in 50 1 m sections, and a sample was cut from the upper end of every second or third core section. A total of 19 such density samples were taken between 9 m and 50 m depth.

During the course of this sampling, it became apparent from measured densities and from examination of the core that there are significant density variations near any given depth. Fine-grained firn which appears dark in transmitted light is relatively dense, while coarse-grained firn which transmits more light is less dense. Layers range from 1 mm to 100 or 200 mm in thickness and are sharply defined.

Sampling was undertaken to determine the maximum density range at a depth. A core section was examined in transmitted light and the two adjacent layers showing the greatest contrast were sampled. This procedure was repeated on every second or third core section from 4 m to 50 m depth. Above 4 m, the core had sublimed and recrystallized to such an extent that proper sampling was deemed impossible.

Subsequently, it was decided to measure densities of entire 1 m sections of core. All core sections were measured except for: 1) Sections from shallower than 12 m. Recrystallization had altered the cylindrical form to such a degree that diameters could not be reproducibly measured. 2) Section 47-48 m, which was already too cut up to be measured. 3) Section 48-49 m, which was missing.

--TIME SCALE

For constant accumulation with only vertical strain, the age of firn at any depth z_o can be calculated by

$$T=\frac{1}{b}\cdot\int_0^{z_o} p\,dz$$

where T=age in years, b=accumulation rate in Mg m^{-2} a^{-1}, p=density in Mg m^{-3}, and z=depth in m.

This may be calculated by smoothing the depth-density profile and fitting a function p=p(z) to the curve, or by

using an approximation of the integral. The latter method was used in this study. The approximation

$$T_i = \frac{1}{b} \cdot \sum_{n=0}^{i} \bar{p}_n \Delta z$$

is introduced, where T_i is the age of firn i meters deep, $\bar{p}_n$ is the average density of the $n^{\underline{th}}$ meter section, and $\Delta z = 1$ m. The average density of each meter section was taken from the depth-density profile, which was smoothed by inspection, and the time required to reach each additional meter depth was calculated. Intermediate values were obtained by linear interpolation.

--CRYSTAL SIZE MEASUREMENT

Crystal size measurement is described in the body of this paper; only a few points need comment.

The scale photographed with each sample allowed easy conversion from measurements on pictures to actual dimensions in the samples. An engineering scale graduated to 1/60" was used to measure dimensions on the pictures. To measure the area of a crystal, a rectangle of the same area was mentally constructed over the crystal, and its length and width were recorded. The area of the crystal on the picture was then calculated. After the average area of 50 crystals in a section was computed, the result was multiplied by the appropriate conversion factor to obtain the mean crystal

area in square millimeters. This method is not as accurate as using a planimeter, but reproducibility is better than $\pm$0.1 mm, and the method is fast and simple.

The crystals measured were selected by inspection. Since this does not guarantee that the largest crystals will be used, a systematic but very small error was introduced.

--SPHERICITY MEASUREMENT

The calculation of sphericity for a sample requires the arithmetic means of the diameters of the largest inscribed and smallest circumscribed circles for a set of crystals. The 55 largest crystals in each sample were measured, as determined by inspection. Calculated sphericities are largely insensitive to whether 50 or 55 crystals are used. The same crystals were used for sphericity and crystal size measurements.

A standard circle template with 20 different circle sizes between 1/16" and 3/8", plus larger sizes, was used to measure the inscribed circles. Different holes and positions of the crystal were tried until the largest circle that could be wholly contained within the crystal was determined. The diameter of that circle was then recorded. It is important to remember that most circle templates have pencil allowances, so that the hole in the template has a larger diameter than the printed value. The diameter of each hole should be

measured as precisely as possible. The actual diameter may be recorded on a strip of tape mounted on the template. This diameter should be recorded with each measurement. It can then be converted to millimeters on the sample with the appropriate conversion factor. The error introduced by the discrete differences between possible inscribed circle diameters should be very minor.

The greatest distance between two points on the perimeter of a crystal was determined by inspection and trial-and-error measuring. This is the diameter of the smallest circumscribed circle.

--SURFACE AREAS

Smith and Guttman (1953) reported that the internal surface area of a three-dimensional network can be calculated by counting the number of intersections of a set of lines, drawn at an arbitrary distance on a random surface through the network, with grain boundaries revealed on that surface.

The plane of section of samples used for this part of the present study was horizontal in all cases. However, the exact position and azimuthal orientation of each sample were not known and are random, which should satisfy the stated requirement. Lines were drawn with ½" spacing in two mutually-perpendicular directions on each picture. The number of times each line intersected a crystal-crystal

boundary or a crystal-pore boundary was recorded. The total crystal-crystal intersections, crystal-pore intersections, and length of line were then calculated for each sample. From these values, internal free surface and crystal boundary were calculated according to the equations given in the body of this paper.

--EVALUATION OF PROCEDURES

The procedures outlined above work. They permit rapid and accurate density and density range determinations, thin section preparation and photography, and crystal size, sphericity, and surface area measurements. The operator can become proficient in a short time. There is little danger from spilled or mishandled chemicals.

However, it would be wrong to claim that these are the best procedures that can be developed. Virtually every phase could be improved upon. In biological microtomy, paraffins are frequently used for mounting samples. However, instead of a single chemical, the microtomist uses a mixture of paraffins specially blended to provide certain desired characteristics. It is possible that other paraffins could be added to the paraffin dodecane to significantly increase its strength without sacrificing its other desirable characteristics. It is also possible that a completely different nontoxic chemical could be

located that would serve better than dodecane. A skilled microtomist, by adjusting knife angle and cutting thickness and carefully sharpening the knife, might find dodecane more than strong enough for rapid sectioning.

Both photographic procedures outlined are time consuming. A way to speed the process while better controlling the temperature would be beneficial.

Other improvements could also be made in methodology. However, the set of procedures outlined above will allow future researchers, here at Ohio State and elsewhere, to safely and efficiently study the density and texture of firn.

APPENDIX B. DENSITY MEASUREMENTS AND TIME SCALE*

TABLE B-1. SMALL DENSITY SAMPLES.

DEPTH (m)	DENSITY ($Mg\ m^{-3}$)	TYPE R=Random C=Coarse F=Fine	DEPTH (m)	DENSITY ($Mg\ m^{-3}$)	TYPE R=Random C=Coarse F=Fine
4.07	0.453	F	24.32	0.577	F
4.16	0.373	C	24.35	0.559	C
7.42	0.414	C	24.37	0.560	C
7.44	0.490	F	26.01	0.544	R
9.01	0.435	R	28.01	0.562	R
9.62	0.457	F	29.01	0.590	R
9.65	0.418	C	29.03	0.592	F
9.68	0.438	C	29.05	0.574	C
11.01	0.453	R	31.01	0.583	R
11.03	0.428	C	34.01	0.604	R
13.01	0.520	F	34.48	0.596	C
13.64	0.461	C	34.50	0.610	F
14.56	0.510	F	36.01	0.601	R
14.58	0.477	C	39.01	0.623	R
14.98	0.480	R	39.29	0.633	F
17.01	0.509	R	39.31	0.623	C
17.48	0.550	F	42.01	0.638	R
17.50	0.490	C	42.02	0.642	F
17.52	0.493	C	42.04	0.638	C
19.01	0.519	R	45.01	0.643	R
19.25	0.540	F	45.16	0.650	F
19.27	0.534	F	45.19	0.640	C
19.29	0.507	C	49.01	0.660	R
21.01	0.528	R	49.07	0.655	C
23.01	0.535	R	49.09	0.658	C
24.01	0.561	R	49.11	0.663	F
24.29	0.547	C			

*All data for Dome C unless otherwise indicated.

TABLE B-2. DENSITY RANGES.

DEPTH (m)	RANGE ($Mg\ m^{-3}$)
4.12	0.080
7.43	0.076
9.65	0.039
13.40	0.059
14.57	0.033
17.49	0.060
19.27	0.033
24.30	0.030
29.04	0.018
34.49	0.014
39.30	0.010
42.03	0.004
45.17	0.010
49.09	0.008

TABLE B-3. DENSITIES OF 1 m SAMPLES.

DEPTH (m)	DENSITY ($Mg\ m^{-3}$)	DEPTH (m)	DENSITY ($Mg\ m^{-3}$)
0-1*	0.355	29-30	0.569
1-2*	0.363	30-31	0.574
2-3*	0.364	31-32	0.592
12-13	0.469	32-33	0.593
13-14	0.480	33-34	0.600
14-15	0.483	34-35	0.610
15-16	0.490	35-36	0.612
16-17	0.490	36-37	0.612
17-18	0.522	37-38	0.618
18-19	0.528	38-39	0.617
19-20	0.517	39-40	0.628
20-21	0.535	40-41	0.636
21-22	0.529	41-42	0.647
22-23	0.535	42-43	0.642
23-24	0.532	43-44	0.644
24-25	0.556	44-45	0.655
25-26	0.560	45-46	0.651
26-27	0.562	46-47	0.661
27-28	0.576	49-50	0.667
28-29	0.574		

*Deep pit data from Palais (1980).

TABLE B-4. SMOOTHED DEPTH-DENSITY PROFILE AND TIME SCALE.

DEPTH (m)	MIDPOINT DENSITY ($Mg\ m^{-3}$)	TOTAL LOAD AT BOTTOM OF SECTION ($N\ m^{-2}$)	TOTAL AGE AT BOTTOM OF SECTION (a)
0-1	0.352	3452	10.4
1-2	0.362	7002	21.0
2-3	0.372	10650	31.9
3-4	0.382	14397	43.2
4-5	0.392	18241	54.7
5-6	0.402	22183	66.5
6-7	0.411	26214	78.6
7-8	0.420	30333	91.0
8-9	0.429	34540	103.6
9-10	0.438	38836	116.5
10-11	0.447	43219	129.6
11-12	0.456	47691	143.0
12-13	0.465	52252	156.7
13-14	0.474	56900	170.6
14-15	0.483	61637	184.9
15-16	0.492	66462	199.3
16-17	0.501	71375	214.1
17-18	0.509	76367	229.0
18-19	0.516	81428	244.2
19-20	0.523	86557	259.6
20-21	0.529	91744	275.1
21-22	0.535	96991	290.9
22-23	0.541	102297	306.8
23-24	0.547	107661	322.9
24-25	0.552	113075	339.1

TABLE B-4 Continued. SMOOTHED DEPTH-DENSITY PROFILE AND TIME SCALE.

DEPTH (m)	MIDPOINT DENSITY (Mg m^{-3})	TOTAL LOAD AT BOTTOM OF SECTION (N m^{-2})	TOTAL AGE AT BOTTOM OF SECTION (a)
25-26	0.557	118537	355.5
26-27	0.562	124049	372.0
27-28	0.567	129609	388.7
28-29	0.572	135219	405.5
29-30	0.577	140878	422.5
30-31	0.582	146585	439.6
31-32	0.587	152342	456.9
32-33	0.592	158148	474.3
33-34	0.597	164002	491.9
34-35	0.602	169906	509.6
35-36	0.607	175859	527.4
36-37	0.612	181861	545.4
37-38	0.617	187912	563.6
38-39	0.622	194012	581.9
39-40	0.627	200161	600.3
40-41	0.632	206359	618.9
41-42	0.637	212606	637.6
42-43	0.641	218892	656.5
43-44	0.645	225218	675.4
44-45	0.649	231582	694.5
45-46	0.653	237986	713.7
46-47	0.656	244420	733.0
47-48	0.659	250883	752.4
48-49	0.662	257375	771.9
49-50	0.665	263897	791.4

TABLE B-5. LOAD-SPECIFIC VOLUME PROFILE CALCULATED FROM SMOOTHED DEPTH-DENSITY PROFILE.

DEPTH (m)	SPECIFIC VOLUME ($m^3\ Mg^{-1}$)	LOAD ($N\ m^{-2}$)	DEPTH (m)	SPECIFIC VOLUME ($m^3\ Mg^{-1}$)	LOAD ($N\ m^{-2}$)
1	2.801	3452	26	1.787	118537
2	2.725	7002	27	1.771	124049
3	2.653	10650	28	1.756	129609
4	2.584	14397	29	1.741	135219
5	2.519	18241	30	1.726	140878
6	2.460	22183	31	1.711	146585
7	2.407	26214	32	1.696	152342
8	2.356	30333	33	1.682	158148
9	2.307	34540	34	1.668	164002
10	2.260	38836	35	1.654	169906
11	2.215	43219	36	1.641	175859
12	2.172	47691	37	1.627	181861
13	2.130	52252	38	1.614	187912
14	2.090	56900	39	1.601	194012
15	2.051	61637	40	1.589	200161
16	2.014	66462	41	1.576	206359
17	1.980	71375	42	1.565	212606
18	1.951	76367	43	1.555	218892
19	1.925	81428	44	1.546	225218
20	1.901	86557	45	1.536	231582
21	1.880	91744	46	1.528	237986
22	1.859	96991	47	1.521	244420
23	1.838	102297	48	1.514	250883
24	1.820	107661	49	1.507	257375
25	1.803	113075	50	1.500	263897

TABLE B-6. SMOOTHED DEPTH-DENSITY PROFILE AND TIME SCALE FOR SOUTH POLE.

DEPTH (m)	MIDPOINT DENSITY ($Mg\ m^{-3}$)	ACCUMULATION ($kg\ m^{-2}\ a^{-1}$)	TOTAL LOAD AT BOTTOM OF SECTION ($N\ m^{-2}$)	TOTAL AGE AT BOTTOM OF SECTION (a)
0-1	0.365	68.8	3580	5.3
1-2	0.382	68.8	7326	10.9
2-3	0.398	68.8	11229	16.6
3-4	0.414	68.8	15289	22.7
4-5	0.428	68.8	19487	28.9
5-6	0.442	65.8	23821	35.6
6-7	0.454	65.8	28274	42.5
7-8	0.465	65.8	32834	49.6
8-9	0.476	65.8	37502	56.8
9-10	0.487	65.8	42280	64.2
10-11	0.497	80.3	47152	70.4
11-12	0.505	80.3	52105	76.7
12-13	0.512	80.3	57126	83.1
13-14	0.519	80.3	62216	89.5
14-15	0.526	74.7	67374	96.6
15-16	0.532	74.7	72591	103.7
16-17	0.538	74.7	77868	110.9
17-18	0.544	74.7	83203	118.2
18-19	0.549	66.8	88587	126.4
19-20	0.554	66.8	94020	134.7
20-21	0.559	66.8	99502	143.0
21-22	0.563	66.8	105023	151.5
22-23	0.567	71.7	110584	159.4
23-24	0.571	71.7	116184	167.3
24-25	0.575	71.7	121823	175.4

TABLE B-6 Continued. SMOOTHED DEPTH-DENSITY PROFILE AND TIME SCALE FOR SOUTH POLE.

DEPTH (m)	MIDPOINT DENSITY (Mg m^{-3})	ACCUMULATION (kg m^{-2} a^{-1})	TOTAL LOAD AT BOTTOM OF SECTION (N m^{-2})	TOTAL AGE AT BOTTOM OF SECTION (a)
25-26	0.579	71.7	127501	183.4
26-27	0.582	64.7	133208	192.4
27-28	0.585	64.7	138946	201.5
28-29	0.588	64.7	144712	210.6
29-30	0.591	75.7	150508	218.4
30-31	0.595	75.7	156343	226.2
31-32	0.598	75.7	162208	234.1
32-33	0.601	75.7	168102	242.1
33-34	0.605	70.8	174035	250.6
34-35	0.608	70.8	179998	259.2
35-36	0.612	70.8	186000	267.9
36-37	0.615	54.7	192031	279.1
37-38	0.619	54.7	198101	290.4
38-39	0.622	54.7	204201	301.8
39-40	0.625	64.7	210331	311.5
40-41	0.628	64.7	216490	321.2
41-42	0.631	64.7	222678	330.9
42-43	0.635	65.0	228905	340.7
43-44	0.638	65.0	235162	350.5
44-45	0.641	65.0	241448	360.4
45-46	0.645	72.5	247774	369.3
46-47	0.648	72.5	254129	378.2
47-48	0.651	72.5	260513	387.2
48-49	0.654	66.7	266927	397.0
49-50	0.657	66.7	273370	406.8

APPENDIX C. CRYSTAL SIZE AND SHAPE PARAMETERS*

TABLE C-1. CRYSTAL CROSS-SECTIONAL AREAS.

DEPTH (m)	TYPE C=Coarse F=Fine	MEAN CRYSTAL AREA (mm^2)	STANDARD DEVIATION	AGE (a)
4.16	C	1.22	0.349	45.0
9.65	C	1.32	0.421	112.0
13.64	C	1.44	0.374	165.4
19.29	C	1.57	0.526	248.7
24.29	C	1.37	0.387	327.6
29.05	C	1.44	0.495	406.4
34.48	C	1.54	0.352	500.4
39.31	C	1.50	0.432	587.6
45.19	C	1.57	0.412	698.2
49.07	C	1.75	0.395	773.3
4.07	F	0.403	0.115	44.0
13.01	F	0.545	0.105	156.9
19.25	F	0.789	0.144	248.1
24.32	F	0.737	0.214	328.1
29.03	F	0.959	0.291	406.0
34.50	F	1.19	0.294	500.7
45.16	F	1.18	0.345	697.6
49.11	F	1.31	0.357	774.0

*All data for Dome C.

TABLE C-2. SPHERICITIES.

DEPTH (m)	TYPE C=Coarse F=Fine	MEAN DIAM. OF MAX. INSCRIBED CIRCLE(M_i) (mm)	STAND. DEV.	MEAN DIAM. OF MIN. CIRCUMSCR. CIRCLE(M_c) (mm)	STAND. DEV.	SPHERICITY M_i/M_c
4.16	C	0.9776	0.189	1.622	0.380	0.6027
9.65	C	0.9542	0.202	1.553	0.414	0.6144
13.64	C	1.062	0.242	1.700	0.405	0.6247
19.29	C	1.088	0.273	1.863	0.499	0.5840
24.29	C	1.037	0.167	1.698	0.354	0.6107
29.05	C	1.093	0.293	1.849	0.537	0.5911
34.48	C	1.055	0.200	1.661	0.304	0.6352
39.31	C	1.047	0.249	1.774	0.500	0.5902
45.19	C	1.152	0.254	1.894	0.325	0.6082
49.07	C	1.237	0.203	2.039	0.458	0.6067
4.07	F	0.6287	0.145	0.9236	0.251	0.6807
13.01	F	0.6613	0.111	0.9786	0.211	0.6758
19.25	F	0.8457	0.142	1.269	0.237	0.6688
24.32	F	0.8265	0.165	1.242	0.301	0.6655
29.03	F	0.9112	0.238	1.385	0.362	0.6579
34.50	F	1.012	0.207	1.562	0.323	0.6479
45.16	F	1.004	0.174	1.586	0.358	0.6330
49.11	F	1.070	0.198	1.656	0.334	0.6461

TABLE C-3. SPECIFIC AREAS.

DEPTH (m)	TYPE C=Coarse F=Fine	CRYSTAL BOUNDARY (Ice-Ice) (m^2/m^3)	INTERNAL FREE SURFACE (Ice-Air) (m^2/m^3)
4.16	C	286.6	2226.2
13.64	C	680.3	1979.4
19.29	C	452.0	1860.5
24.29	C	786.8	1606.7
29.05	C	437.8	1463.1
34.48	C	720.0	1749.4
39.31	C	860.1	1526.3
45.19	C	639.2	1341.0
49.07	C	1030.8	1044.7
4.07	F	594.8	4185.7
13.01	F	626.7	3216.1
19.25	F	955.6	1978.6
24.32	F	866.9	2191.0
29.03	F	1037.6	1715.0
34.50	F	900.5	1710.9
45.16	F	897.5	1426.0
49.11	F	958.8	1306.5

APPENDIX D. SUGGESTED ADDITIONAL STUDIES

During the course of this investigation, a number of interesting results arose which could not be pursued because of time limitations. Some of these are presented below, in the hope that other investigators, here at Ohio State or elsewhere, will pursue them. Some are ideally suited for senior thesis projects.

I. Crystal Shape Orientation.

A thin section was prepared in the vertical plane of a coarse layer from 4.16 m depth. Inspection of the section revealed that there was a preferred vertical orientation of the long axes of the ice crystals. The angular orientation of the crystals was then measured. For crystals which approximated rectangles, the orientation of one of the long sides was measured; for crystals which resembled ellipses, the orientation of the major axis was used; for the relatively few equant crystals, no measurements were taken. The results of these measurements are plotted on the rose diagram in figure D1. 90° is vertical orientation, and full scale is 24 crystals. A total of 158 crystals was measured.

The microtome stroke used in preparing this section was curved, varying from 90° to 135°. If it were causing the preferred orientation, the maximum would occur at about 112°

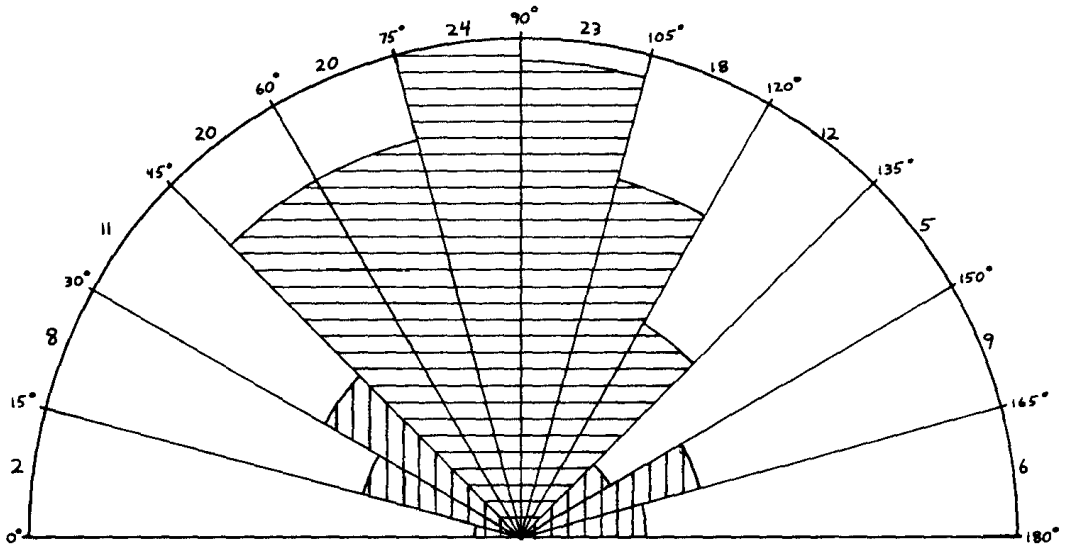

figure D1

ORIENTATION OF MAJOR CRYSTAL AXES IN VERTICAL SAMPLE FROM 4m DEPTH

90° = Vertical

Number of crystals falling in a sector is indicated at the end of that sector.

Number of crystals in each sector is plotted from the center. Radius = 24 crystals.

instead of 90°. Furthermore, a second section was prepared with the cut varying from 0° to 45°, and a maximum was still obtained at 90°. Thus, it seems probable that the preferred orientation exists in the ice sheet, and is not an artifact of the sectioning procedure.

This is not surprising. Temperature gradients in firn are insignificant horizontally over a distance of kilometers, but significant vertically over a distance of meters. Thus, vertical air movements occur in the region of temperature gradients (roughly, the upper 10 m). These air movements transport water vapor, leading to the preferred orientation.

Many questions remain to be answered. Are preferred orientations limited to coarse layers, or do they occur in fine layers as well? How do preferred orientations vary with depth? By what mechanism are they destroyed (a cursory examination of a vertical section from 24 m revealed no preferred orientation)?

A method employed by Narita and others (1978) for the preparation of thin sections could prove useful in such a study. They recognized that all organic fillers commonly used in sectioning are not as strong as ice. Where easy and rapid sectioning are important, and minor alteration of crystals is acceptable, chilled water stained with blue food coloring may be used as a filler. If enough food coloring

is used, the filled pores will appear dark in transmitted light. If the water used is close to freezing, little alteration of crystals should occur, and that alteration should not affect the observed crystal orientation.

II. Crystallographic Orientation.

Data on crystallographic orientations have been collected from many locations, but not from Dome C. Such a study could prove informative, and could be readily conducted using samples already in the IPS cold room. Chilled water with blue dye would make a good filler for such a study.

III. Largest Crystals.

In each thin section a few crystals were observed which were significantly larger than the observed mean size. Table D-1 contains data on the largest observed crystal in each section. The standard deviation was calculated for the 50 crystals following the 5 largest crystals.

It is interesting to note that, while neither is an extremely good fit, the least-squares regression lines for the largest crystal size versus age for coarse-grained firn and for fine-grained firn reveal growth rates of 3.02×10^{-3} mm^2 a^{-1} and 3.05×10^{-3} mm^2 a^{-1} respectively. The similarity of these values is notable, as is the fact that

TABLE D-1. LARGEST CRYSTALS.

DEPTH (m)	TYPE C=Coarse F=Fine	MEAN CRYSTAL AREA M (mm^2)	STAND. DEV. S	LARGEST CRYSTAL AREA L (mm^2)	DIFF. (L-M) (mm^2)	DIFF. IN STAND. DEVS. (L-M)/S (mm^2)
4.16	C	1.22	0.349	2.50	1.28	3.67
9.65	C	1.32	0.421	3.94	2.62	6.22
13.64	C	1.44	0.374	2.96	1.52	4.06
19.29	C	1.57	0.526	4.96	3.39	6.44
24.29	C	1.37	0.387	2.62	1.25	3.23
29.05	C	1.44	0.495	6.13	4.69	9.47
34.48	C	1.54	0.352	4.22	2.68	7.61
39.31	C	1.50	0.432	4.45	2.95	6.83
45.19	C	1.57	0.412	4.42	2.85	6.92
49.07	C	1.75	0.395	5.59	3.84	9.72
4.07	F	0.403	0.115	1.40	0.997	8.67
13.01	F	0.545	0.105	1.47	0.925	8.81
19.25	F	0.789	0.144	1.82	1.03	7.16
24.32	F	0.737	0.214	2.10	1.36	6.37
29.03	F	0.959	0.291	3.15	2.19	7.53
34.50	F	1.19	0.294	2.45	1.26	4.29
45.16	F	1.18	0.345	3.64	2.46	7.13
49.11	F	1.31	0.357	3.06	1.75	4.90

they exceed the observed growth rate for fine-grained firn by a factor of about 2.5, and of coarse-grained firn by a factor of 7.2.

The statistical significance of this observation is open to debate, especially since there is no systematic increase in the number of standard deviations by which the largest crystal exceeds the mean with age. However, it is an observation which deserves a more thorough empirical and theoretical study.

IV. Theory.

Although many excellent studies have been executed, no unified theory exists which completely explains all of the observed phenomena of densification and recrystallization for coarse-grained and fine-grained firn. It is not even clear that enough data have been collected in a systematic manner to allow the construction of such a theory.

Effort should be directed to collecting further data related to this problem, and to fabricating a complete theory of the transformation of snow to firn and then to ice.